Study of Rydberg EIT and its Applications Towards Squeezing and Microwave Interferometry

A Thesis Submitted in partial fulfillment of
the requirements for the Degree of
Bachelor of Science (Research)
In the Faculty of Science

Submitted By
Sambit Banerjee

Supervisor
Prof. Vasant Natarajan
Prof. Patrick Windpassinger

Undergraduate Programme
Indian Institute of Science
Bangalore – 560012
May 2019

Declaration of Authorship

I, Sambit Banerjee, declare that this thesis titled, 'Study of Rydberg EIT and its Applications Towards Squeezing and Microwave Interferometry' and the work presented in it are my own. I confirm that:

- This work was done wholly while in candidature for the Bachelor of Science (Research) degree at the Indian Institute of Science.
- No part of this thesis has previously been submitted for a degree or any other qualification at any other institution.
- Where I have consulted the published work of others, this is always clearly attributed.
- I have acknowledged all main sources of help.

Sambit Banerjee
UG Programme
Indian Institute of Science
Bangalore–560012

To,
My parents, to whom I owe most of what I have achieved in life, and who have been my biggest support throughout.

Acknowledgement

As is true for most original pieces of work, this research work was not brought together by me alone, and the almost innumerable times that I have been helped and guided by several people at several stages warrants a mention of as many of them as possible. Indeed, I have learnt a lot over the past one year or so, and hopefully matured as a researcher working in atomic physics. This has not been due to only reading books and articles and papers, but largely because of very insightful discussions that I had with several people about a plethora of things, and the hands-on training I have received from my lab seniors.

Firstly, I must thank Prof. Vasant Natarajan, Dept. of Physics, Indian Institute of Science, Bangalore, for agreeing to be my faculty advisor and giving me the opportunity to work in his lab as well as to get the exposure of working abroad in Mainz. He is indeed a wonderful human being, and of course, needless to say, extremely knowledgeable about both the theoretical and experimental aspects of physics. He has been a constant guide at different stages and helped me out with various decisions, including but not limited to just the experiments I performed. I must also thank the professors I have worked with previously, and whose courses I have taken, especially Prof. Ambarish Ghosh, who have immense contribution in helping me obtain the limited knowledge in physics that I have, and who have helped shape the way I think.

Secondly, I must thank Prof. Patrick Windpassinger, for accepting me in his lab group and agreeing to fund me for the extended period of seven months. I must admit that the resources available in India fall short by quite an extent compared to what were available to me at Mainz and the opportunity to work there really helped me grow as a researcher. Being able to work on cutting-edge physics reignited my interest in research and helped me grow as a person. Patrick (as I have come to call him after a lot of getting used to the fact that professors *are* called on first name basis in Germany) was a wonderful PI and the SIF meetings really helped give me perspective and chalk out my directions in the project. Patrick was always full of ideas, and his immense experience and knowledge was very apparent whenever we discussed our projects with him. He was always a very good guide and helped me a lot with my decisions regarding my future studies.

I can never really thank my lab seniors enough for all the help I have received from them. This doesn't just include help in experiments. Discussions with my lab seniors have taught me how to think and have given me a lot of intuition at various levels. I must mention a few names here. At Mainz, Parvez was my immediate supervisor and we have worked together for the experiment. He was really helpful and always helped me plan out the next step in the experiment, apart from helping me update my knowledge about the various facets of the research problem at every step. I also had very insightful discussions with Wei, who also taught me a lot of lab techniques and procedures. Noaman and Maria were the really experienced people in the SIF group and their knowledge was really unparalleled. They were the go-to people in case nothing worked and all the ideas that me, Parvez or Wei had come up with had failed. I also learnt a lot from my interactions with all the other lab members- Niels, Pierre, Florian, Marcel, Moritz, Andre, Hu Di, Soren, Ronja, Gunter, Christian and Jonas. I made some really good friends and had a gala time in Mainz. I must also thank Elvira for helping me with all the logistical details of my stay in Mainz, including but not limited to finding a place to stay in. I must thank Mr. and Mrs. Fricke for being a wonderful landlord and landlady, and Golokesh, Mohammad and Tarekh for being amazing roommates.

At IISc, I must thank Mangesh for helping me out with most of the problems that I face on a day-to-day basis. He has a very deep knowledge about AMO physics and he is an amazing teacher. He can explain a very complicated physical phenomenon wonderfully with just qualitative reasoning and a deep intuition. I must also thank Sumanta for helping me out with my experiment, especially the theoretical parts, and for teaching me LaTeX and helping me with my entire thesis. He is the senior-most member of our lab at the moment and the most experienced. A lot of the theory portions have been inspired from his PhD thesis. I must also thank Pritam, my UG senior in the lab, for being the "best senior" (as he likes to call himself), and helping me out with various things related to my experiment and thesis. I should also thank Pooja and Kavita for insightful discussions regarding my experiment. These people have all become wonderful friends of mine over the past few months, or rather since I first did my summer project in Vasant sir's lab. I must also thank Raghuveer Sir for taking care of all the logistics in the lab. I also thank all my lab members from my previous projects, especially Pranay from Ambarish Sir's lab, who have all contributed to my limited experimental skill and knowledge.

Of course, it's not possible to talk about everyone in this small acknowledgement. I think I have made some lifelong friends at IISc, who are more like family now. Rhythmica and the table tennis club have provided me the much needed break from studies at IISc. And last but not the least, I am thankful to my parents and my family, who are the reason I am where I am now.

Abstract

In this thesis, we have studied the phenomenon of electromagnetically induced transparency (EIT) using Rydberg levels of ^{87}Rb. Rydberg levels are unique because they can be described using a hydrogen-like model with the valence electron in an almost circular orbit. Atoms in these levels have long lifetimes and high dipole moments compared to low-lying levels. The values of the principal quantum number n is typically more than 30. The probe laser is locked to the $F_g = 2 \rightarrow F_e = 3$ hyperfine transition of the 780 nm D_2 line of ^{87}Rb. The control laser couples transitions of the $5P_{3/2}$ state of ^{87}Rb to a Rydberg level, and has also been locked. The laser is at 480 nm and values of n up to 95 have been studied. We have used Rydberg EIT to study two things—quadrature squeezing and the effect of an external electromagnetic field. We have employed a balanced homodyne detection scheme to look for probable squeezing of the probe beam emerging out of a Rydberg EIT after passing through the so-called “Rydberg blockade”. In the shot-noise limited regime, we have obtained preliminary results that show phase-dependent noise fluctuations. The effect of an external electromagnetic field has also been used for preliminary studies on microwave interferometry using Rydberg levels in an atom.

Contents

List of Figures

1

Introduction

1.1 Thesis overview

This thesis comprises of the work done at the Johannes Gutenberg University, Mainz, Germany in the group of Prof. Patrick Windpassinger from May 15-December 15, 2018, and the work done at the Indian Institute of Science, Bangalore, India, in the group of Prof. Vasant Natarajan from January 2-April 14, 2019. The problems I have worked on are both based on atomic coherences in $^{8}7$Rb, but the end results expected are quite different. In Mainz, my work was focused on exploring the nonlinearities associated with Rydberg atoms, obtained by excitation following an EIT pathway[1]. In particular, it was focused on building a homodyne detector for measuring probable squeezed states of light obtained from Rydberg atoms. In IISc, my work is focused on the more fundamental aspects of the EIT phenomenon. In particular, we want to use the fact that a Rydberg atom is highly sensitive to external electric fields and that the EIT peak splits when subjected to external fields. Using the above observation, we want to carry out microwave interferometry using Rydebrg EIT, a theoretical background of which has already been given [2].

The chapters are arranged to provide a brief but systematic theory. Chapter 2 deals with two level systems, the density matrix formalism, Bloch equations and EIT. Some portions of Chapter 2 have been inspired from previous bachelor and PhD theses from the Natarajan lab at IISc, especially from the PhD thesis of Sumanta Khan [3] and the bachelor thesis of Pritam Priyadarsi [4], and from some books[5][6]. This is a chapter that serves as a foundation of all the atomic physics we have used in our experiments. Chapter 3 focuses on the quantisation of the EM field in free space, coherent and Fock states, squeezed states, homodyne detection and nonlinearities arising from Rydberg blockade. For the initial sections, I have followed a few textbooks in the field of quantum optics [7] [8]. Basically, it is the foundation for everything related to quantum light that we have used in our experiment. Again, I have tried to make it as succinct as possible. Then we move on to chapter 4. It is a compilation of the experimental details and the results we have got towards getting EIT signals at high n states, and towards obtaining squeezed light from the Rydberg blockade and detecting it by a balanced homodyne detection scheme.

1.2 Applications of different n levels in Rydberg atoms for microwave interferometry

The Rydberg EIT can be used for various kinds of precision experiments. Due to its sensitivity to external electric fields, Kanhaiya Pandey *et al* have recently proposed methods to utilise a loopy ladder type system (Fig. 1.1) to carry out Rydberg based microwave interferometry [2]. The above figure has been taken from the aforementioned

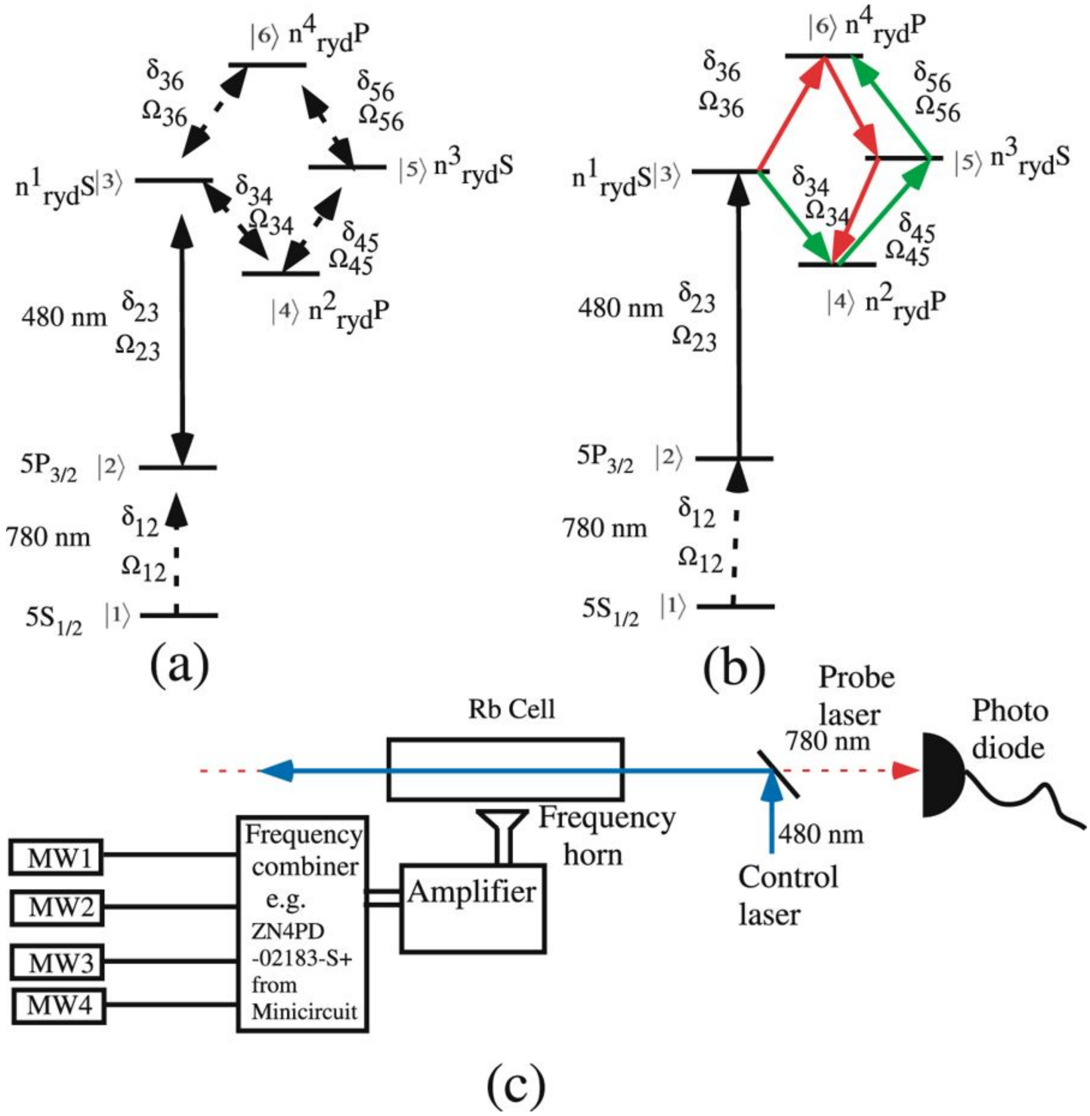

Figure 1.1: Schematic of the proposed setup, employing four Rydberg levels, with microwaves coupled to transitions between them.

paper. For this method to work, one would need to couple three different microwave fields to three different transitions between Rydberg levels, with control over the frequency and phase of the microwaves. The initial Rydberg level would be coupled to laser fields by an EIT scheme. The paper shows that if such a system can be acheieved, one can measure a fourth unknown microwave field with unprecedented precision from the splittings of the Rydberg EIT because of external fields. The four transitions are selected to complete the loopy ladder system. The splitting would happen because of alternate EITATA... where there would be alternate transparencies and absorptions.

1.3 Exploring nonlinearities and non-classical light generation from the Rydberg blockade

Rydberg excitations in alkali atoms have been of considerable interest in the past decade or so. Due to the electrons occupying high n states, Rydberg atoms have a very high dipole moment between this excited electron and the positively charged nucleus. This leads to very interesting effects arising from strong dipole-dipole interactions. Many former papers have shown the formation of the Rydberg blockade due to Rydberg excitations [9][10][11][12]. Due to Van der Waals potential arising from the Rydberg atom, the surrounding atoms upto a certain radius of influence cannot show two photon Rydberg excitations, or the Rydberg EIT transition to a Rydberg state from a first excited state. This forms what are called "dark state polaritons"[13]. Various papers have also explored the nonlinearities arising from Rydberg excitations, inside this Rydberg blockade[10][11][12].

One way in which one can control the Rydberg transition and obtain tunable effects is through the phenomenon of the Rydberg Electromagnetically Induced Transparency (EIT). People have obtained Rydberg EIT in a vapour cell as early as 2007[14]. Since then, many people have demonstrated the Rydberg EIT and utilised it for various purposes. Recently, there is a drive towards exploring and exploiting Rydberg transitions for quantum simulation. Rydberg EIT with laser cooled atoms trapped in a MOT have proved to induce non-classical and non-linear effects like photon bunching and anti-bunching [15]. The "Strong Interaction in Hollow Core Fibers" group in Mainz intends to utilise such non-classical effects from the Rydberg EIT for quantum simulation as well. In order to do so, the SIF group uses a hollow core fiber as a confining medium for atom-light interactions. In this setup, Rb atoms are first trapped in a 2D MOT. Then a pushing beam is used, and the cooled atoms (temperature is a few K), after being trapped in a 3D MOT at the mouth of the fiber, are loaded into a dipole trap [16] conveyer belt [17] [18] [19]. For the conveyer belt, two beams are aligned with a slight frequency detuning between them, from the two ends of the HCF. This creates an optical lattice, famously known as the 'pancake lattice', and the relative detuning can be controlled to move the optical lattice in a certain direction with a certain speed. Rydberg EIT inside the hollow-core photonic crystal fiber (HCPCF) has already been

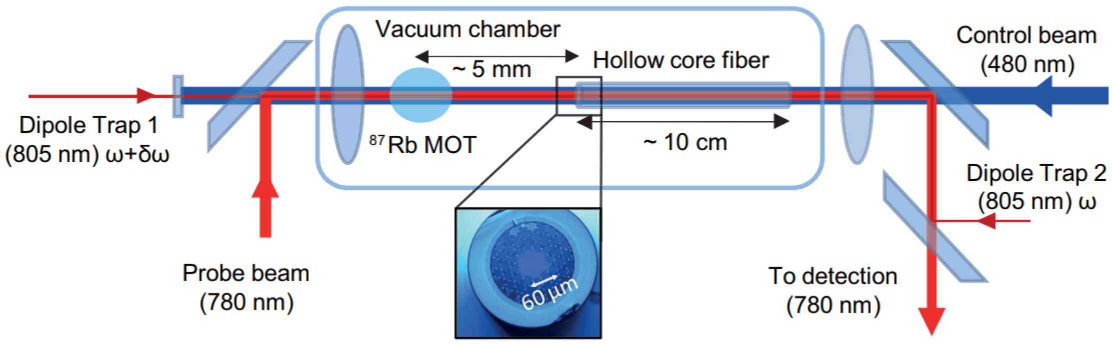

Figure 1.2: Schematic of the hollow core fiber setup in Mainz.

demonstrated for the first time ever in our lab by my seniors [20]. The schematic is shown above in Fig. 1.2 from the cited paper. The Rydberg EIT creates Rydberg polaritons, which are light-matter quasiparticles with a certain blockade radius, and do not absorb photons of the control beam which leads to the Rydberg transition, in the blockade volume. The lab intends to use the non-linear nature of the Rydberg EIT to observe photon-photon interactions and non-classical states of light, and later use them for quantum information. Given this general long-term goal, it is prudent that one investigates and detects non-classical light states from the system. Given the non-linear nature of the phenomenon, we expect to detect some squeezing of the emerging probe beam from the Rydberg EIT medium. In order to detect so, it was required that one builds a homodyne detector[21], primarily to detect squeezing from Rydberg EIT, and for quantum state tomography of Rydberg EIT in general. This was what my project was all about. I built a homodyne detector for detection of squeezing, more specifically squeezing of the EIT probe beam, in thermal Rb vapour, and then I characterised the setup. Although squeezed light has been used in association with EIT for various applications [22]][23][24], and squeezing has been produced from atoms by nonlinear processes like 4-wave mixing [25], to the best of my knowledge, Rydberg BLockade-induced squeezing has never been reported. We have obtained preliminary signs of phase dependent fluctuations of the shot noise level of the probe beam emerging from a Rydberg EIT. Whether this is squeezing indeed or not, is under further investigation.

2

Atomic coherences and quantum interference

In this chapter, we will mostly use a semi-classical treatment of atom-light interactions. We treat the light field as a classical electromagnetic field and the atom as a quantum system with discrete energy levels. I shall not digress into Time-Dependent Perturbation Theory but take the liberty to use techniques and results that arise from the theory in my thesis, wherever required.

2.1 Density matrix formalism and equations of motion of the density matrix

A very common formalism to analyse an atomic system is the density matrix formalism. Ideally, the complete description of an atomic state is given by the wavefunction $|\psi\rangle$. However, $|\psi\rangle$ can't be measured directly in an experiment. The average value of a measurement usually yields an expectation value of an observable $\hat{A}$ (which is usually a Hermitian operator) as

$$\langle \hat{A} \rangle = \langle \psi | \hat{A} | \psi \rangle \tag{2.1}$$

where $|\psi\rangle$ is the normalised wave function. Define a density operator ρ for a pure state as

$$\rho = |\psi\rangle \langle \psi| \tag{2.2}$$

For an n-dimensional Hilbert space, the density matrix for a state with basis expansion as $|\psi\rangle = \sum_{i=1}^{n} c_i |x_i\rangle$ is given by

$$\rho_{ij} = \langle x_i | \rho | x_j \rangle \tag{2.3}$$

and the normalisation for the wave function yields $\mathrm{Tr}(\rho) = 1$. The diagonal terms give the probability of an atom to be in some state $|x_i\rangle$ while the off-diagonal terms are called coherences. Coherences represent the relative phase-differences between the various off-diagonal entries. Now, we can write

$$\langle \hat{A} \rangle = \sum_{i,j} c_i^* c_j \langle x_i | A | x_j \rangle = \sum_{i,j} \rho_{ji} A_{ij} = \sum_j (\rho A)_{jj} = \mathrm{Tr}(\rho A) \tag{2.4}$$

For a mixed state, the probabilities of being in a certain state comes into the picture and the density matrix equations, especially the trace, can be used as a test for determining whether a state is pure or mixed.

Our main target in this section is to arrive at a tool for understanding the time evolution of a density matrix and for providing a theoretical framework for interesting effects like EIT and EIA that we observe in atoms interacting with a laser radiation. For this, let us first look at the time evolution of a density matrix and then try to relate something as abstract as a density matrix to something which influences our experimental measurements, like susceptibility of a medium.

A density matrix follows the below time evolution in terms of the Hamiltonian, which is something we need to first define for analysis of any atomic system

$$\dot{\rho} = -\frac{\mathrm{i}}{\hbar}[H, \rho] \tag{2.5}$$

This equation is called the Liouville equation. However, this is rather incomplete in the sense that we have not considered any decoherence terms in this expression, or any terms that actually correspond to a physical atomic process. For this, we define two matrices, namely the **relaxation matrix** and the **repopulation matrix** to account for atomic decay rates and repopulation rates, which arise to conserve the number of atoms while being subjected to some decay process due to various interactions with the external environment. The decay might occur due to various reasons like spontaneous emission or atomic collisions, which corroborates with the fact that atomic transitions have a finite lifetime. The relaxation matrix Γ is given by

$$\langle x_i | \Gamma | x_j \rangle = \Gamma_i \delta_{ij} \tag{2.6}$$

Note that the above defined matrix is completely phenomenological, as in, the explicit expression of the terms come from experimental observations. For every relaxation process, there has to be a repopulation term, to make sure that the total number of atoms is conserved. Let this be given by the repopulation matrix $(\dot{\rho})_{repop} = \Lambda$. So, the final Liouville Equation for density matrix time evolution becomes

$$\dot{\rho} = -\frac{\mathrm{i}}{\hbar}[H, \rho] - \frac{1}{2}\{\Gamma, \rho\} + \Lambda \tag{2.7}$$

where $\{\Gamma, \rho\}$ is the anticommutator.
Then the ij-th matrix element of the Liouville equation becomes

$$\dot{\rho_{ij}} = -\frac{\mathrm{i}}{\hbar} \sum_k (H_{ik}\rho_{kj} - \rho_{ik}H_{kj}) - \frac{1}{2} \sum_k (\Gamma_{ik}\rho_{kj} + \rho_{ik}\Gamma_{kj}) + \Lambda_{ij} \tag{2.8}$$

Now let us try to relate the density matrix with the polarisation and susceptibility of the medium. As we know, when light propagates through a medium, it polarises the atoms in the medium. The polarisation P can be found from the density matrix as the expectation value of the dipole operator d.

$$P = nTr(\rho d) = n\sum_{i,j}\rho_{ji}d_{ij} \tag{2.9}$$

Polarisation P in terms of the susceptibility χ of the medium can be written as

$$P = \frac{1}{2}\epsilon_0\varepsilon(\chi(\omega) + c.c.) \tag{2.10}$$

where ε is the electric field. Then, we can relate χ to the density matrix as

$$\chi = \frac{2nd_{ij}}{\epsilon_0\varepsilon}\rho_{ji} \tag{2.11}$$

2.2 Optical Bloch equations and two-level systems

We can express the wave function for two levels $|1\rangle$ and $|2\rangle$ as

$$|\psi\rangle = c_1(t)\,|1\rangle + c_2(t)\,|2\rangle\, e^{-\mathrm{i}\omega_0 t} \tag{2.12}$$

After solving the Schrödinger's equation for a two-level system, and doing the dipole approximation and the Rotating Wave Approximation, we get-

$$\mathrm{i}\hbar\dot{c_1(t)} = c_2(t)\hbar\Omega\frac{e^{\mathrm{i}\Delta t}}{2} \tag{2.13}$$

$$\mathrm{i}\hbar\dot{c_2(t)} = c_1(t)\hbar\Omega\frac{e^{-\mathrm{i}\Delta t}}{2} \tag{2.14}$$

Where $\Delta = \omega - \omega_0$ is called the detuning. We define the Rabi frequency as follows

$$\Omega = \frac{E_0}{\hbar}\langle 2|\,\vec{\mu}.\hat{E}\,|1\rangle \tag{2.15}$$

If μ_{12} is the dipole moment of a certain transition, we can write the Rabi frequency as

$$\Omega = \frac{E_0}{\hbar}\mu_{12} \tag{2.16}$$

Equations (2.13) and (2.14) indicate that the ground state and the excited state populations will continuously change and some sort of population oscillation will set in when a light field is made incident on atoms. Differentiating equations (2.13) and (2.14) and substituting the initial equations (2.13) and (2.14) in the obtained 2^{nd} order differential equation gives two uncoupled 2^{nd} order differential equations as below

$$\frac{d^2c_1}{dt^2} - \mathrm{i}\Delta\frac{dc_1}{dt} + \frac{\Omega^2}{4}c_1 = 0 \tag{2.17}$$

$$\frac{d^2c_2}{dt^2} + \mathrm{i}\Delta\frac{dc_2}{dt} + \frac{\Omega^2}{4}c_2 = 0 \tag{2.18}$$

We assume an oscillatory solution to these and obtain

$$|c_2(t)|^2 = \left(\frac{\Omega}{W}\right)^2 \sin^2[Wt/2] \tag{2.19}$$

where $W = \sqrt{\Omega^2 + \Delta^2}$. These oscillations are called **Rabi oscillations**. When the applied laser field is on resonance with the exact transition frequency, Δ is zero. Then the transition probability is given by

$$|c_2(t)|^2 = \sin^2[\Omega t/2] \tag{2.20}$$

From this expression it is clear that a "π pulse", that is, a temporal pulse of duration π/Ω and frequency same as resonant frequency of transition, will lead to the atom ending up in the state $|2\rangle$ after being subjected to the pulse. Thus, this is like a swapping of the ground and excited states. A "$\pi/2$ pulse" will, on the other hand, prepare the atom in a superposition state with equal amplitudes of the ground and excited states.

After this short discourse on two-level systems, let me just briefly mention what are the Optical Bloch Equations, which are extensively used in the analysis of any system where quantum interference plays a dominant role, like EIT and EIA processes, which form a central part of my experiments. The density matrix for a two-level atomic system is given by

$$\rho = \begin{bmatrix} \rho_{11} & \rho_{12} \\ \rho_{21} & \rho_{22} \end{bmatrix} \tag{2.21}$$

Assume that each level undergoes relaxation at a rate γ due to the exit of atoms from the light beam (depends on the beam width and the velocity of atoms at that temperature). In addition, the upper state $|2\rangle$ undergoes spontaneous decay at a rate Γ_2. The relaxation matrix is then given by

$$\Gamma = \begin{bmatrix} \gamma & 0 \\ 0 & \gamma + \Gamma_2 \end{bmatrix} \tag{2.22}$$

To conserve the total population, the repopulation matrix becomes

$$\Lambda = (\gamma + \Gamma_2\rho_{22}) \begin{bmatrix} 1 & 0 \\ 0 & 0 \end{bmatrix} \tag{2.23}$$

Under Rotating Wave Approximation (RWA), we can write the Hamiltonian for a 2-level system as

$$\tilde{H} \simeq \frac{\hbar}{2}\begin{bmatrix} -\Delta & \Omega_{12} \\ \Omega_{21} & \Delta \end{bmatrix} \tag{2.24}$$

Now, using Eqns. (2.21)-(2.24), and using the Liouville Equation, we get what are called the **Optical Bloch Equations**.

$$\begin{aligned}
\dot{\rho_{11}} &= \frac{\mathrm{i}}{2}(\Omega_{21}\rho_{12} - \Omega_{12}\rho_{21} - \gamma\rho_{11} + \Gamma_2\rho_{22} + \gamma \\
\dot{\rho_{22}} &= \frac{\mathrm{i}}{2}(\Omega_{12}\rho_{21} - \Omega_{21}\rho_{12} - (\gamma + \Gamma_2)\rho_{22} \\
\dot{\rho_{12}} &= -\left(\gamma + \frac{\Gamma_2}{2} - \mathrm{i}\delta\right)\rho_{12} + \frac{\mathrm{i}}{2}\Omega_{12}(\rho_{11} - \rho_{22}) \\
\dot{\rho_{21}} &= -\left(\gamma + \frac{\Gamma_2}{2} + \mathrm{i}\delta\right)\rho_{12} - \frac{\mathrm{i}}{2}\Omega_{12}(\rho_{11} - \rho_{22})
\end{aligned} \tag{2.25}$$

These equations are exactly the same as the Liouville Equation, but just with each element of the matrices written in an equation form, following Eqn. (2.8). A slightly different but more compact representation of the density matrix time evolution is also given by the Lindblad Equation [26].

2.3 AC Stark shift, dressed state picture and hyperfine structure

We can find the energy eigenstates of the Hamiltonian given in Eq. (2.24) and subsequently the energy eigenvalues in the uncoupled energy basis by diagonalising the Hamiltonian. These are given by

$$E_{\pm} = \pm\frac{\hbar}{2}\sqrt{|\Omega_{12}|^2 + \Delta^2} \tag{2.26}$$

The eigenvectors are given by an effective rotation of the uncoupled basis states $|2\rangle$ and $|1\rangle$ as,

$$\begin{bmatrix} |+\rangle \\ |-\rangle \end{bmatrix} = \begin{bmatrix} \sin\theta & \cos\theta \\ \cos\theta & -\sin\theta \end{bmatrix} \begin{bmatrix} |1\rangle \\ |2\rangle \end{bmatrix} \tag{2.27}$$

where $|\pm\rangle$ are called dressed states—eigenstates of the combined light-atom system—and the Stückelberg angle θ defined as

$$\tan 2\theta = \frac{\Omega_{12}}{\Delta}(0 \leqslant \theta < \pi/2) \tag{2.28}$$

The energy shift, called the **AC Stark Shift**, far from resonance, that is, $\Omega_{12} << \Delta$, is given by

$$\Delta E = \frac{\hbar\Omega^2}{4\Delta} \tag{2.29}$$

Now I shall very briefly describe the hyperfine structure of atoms and then we shall discuss in some detail the phenomenon of EIT.

The magnetic moment of nucleus associated with nuclear spin $\boldsymbol{I}$ is given by

$$\boldsymbol{\mu_I} = g_I \mu_N \boldsymbol{I}/\hbar \tag{2.30}$$

where g_I is the (dimensionless) nuclear Lande factor specific to the particular nucleus and μ_N is nuclear magneton given by

$$\mu_N = \frac{e\hbar}{2m_p c} = \frac{\mu_B}{1836} \approx 762\text{HzG}^{-1} \tag{2.31}$$

where μ_B= 1.4 MHz/G is the Bohr magneton. Clearly, the nucleus-electron interaction is very weak compared to the electron-electron Coulomb interaction. This interaction causes the fine structure levels to split by a very small magnitude to form Hyperfine levels.

As the nuclear magnetic moment couples with the magnetic field, the nuclear spin also couples to the total electronic angular momentum to give the total angular momentum $\boldsymbol{F}$.

$$\boldsymbol{F} = \boldsymbol{I} + \boldsymbol{J} \tag{2.32}$$

$\boldsymbol{F}$ can take the values

$$|J - I| \leq F \leq J + I \tag{2.33}$$

The hyperfine interaction energy is given by the magnetic coupling between $\boldsymbol{I}$ and $\boldsymbol{J}$ as

$$W_{\text{hfs}} = -\mu_I \cdot B_J \tag{2.34}$$

Of course, this energy splitting is less than the fine structure, but it is usually observable for isotopes that have a nuclear spin. Now to calculate the hyperfine structure energy, we have to calculate B_J. It is usually proportional to $\boldsymbol{J}$ and is given by

$$\boldsymbol{B_J} = \frac{a}{\mu_N}\boldsymbol{J}/\hbar \tag{2.35}$$

So the hyperfine structure energy is

$$W_{\text{hfs}} = A\boldsymbol{I}.J/\hbar^2 \tag{2.36}$$

where A is the magnetic dipole hyperfine coupling constant. The energy shift for a state with quantum numbers F , I , and J is

$$\Delta E_{\text{hfs}} = A\frac{F(F+1) - I(I+1) - J(J+1)}{2} \tag{2.37}$$

Hyperfine energy can be expanded in a multipole series with progressively smaller correction as

$$W_{\text{hfs}}^{\text{total}} = AK_1 + BK_2 + CK_3 + DK_4 + \dots \tag{2.38}$$

where B is the electric quadrupole hyperfine coupling constant, C is the magnetic octupole hyperfine coupling constant, D is the electric hexadecapole hyperfine coupling constant, and so on. K's are factors that depend on the quantum numbers of the state. The lowest term of the series are dominant which are magnetic dipole and electric quadrupole interactions between nucleus and the electrons. The dipole matrix elements between hyperfine levels can be calculated by using Wigner $3-j$ symbol (written within round brackets) or equivalently Clebsch-Gordan coefficient and Wigner $6-j$ symbol (written within curly brackets) as follows

$$\begin{aligned} \left\langle \xi' F' m_F' \left| d_{\pm 1}^1 \right| \xi F m_F \right\rangle &= (-1)^{F'-m_F'} \begin{pmatrix} F' & 1 & F \\ -m_F' & \pm 1 & m_F \end{pmatrix} \times \left\langle \xi' F' \left\| d^1 \right\| \xi F \right\rangle \\ &= (-1)^{F'-m_F'} \begin{pmatrix} F' & \pm 1 & m_F \end{pmatrix} \times (-1)^{(J'+I+F+1)} \\ &\times \sqrt{(2F'+1)(2F+1)} \begin{Bmatrix} J' & F' & I \end{Bmatrix} \left\langle J' \left\| d^1 \right\| J \right\rangle \end{aligned} \tag{2.39}$$

The double bar represents a reduced matrix element.

2.4 Electromagnetically induced transparency

EIT is caused by the quantum interference of excitation pathways in a certain atomic configuration. The laser field incident on the atoms give rise to coherence of the atomic states, and the lasers can be used to control the optical response of the medium. So, there are many interesting effects that arise like EIT, EIA, CPT, LWI, STIRAP, etc. We shall focus on EIT in this section, which is what most of our work is based on. EIT has many applications as it effects in a highly nonlinear susceptibility in the transparency window, and also shows a steep dispersion. This makes it an ideal candidate for experiments on slow light, light storage, precision interferometry, and, as has been discussed in a later part of the thesis, on utilization of the induced nonlinearity.

EIT can be described experimentally as a process in which a strong control beam and a weak probe beam overlap with each other in an atomic medium (might be a vapour cell or a cold atom system), and the frequencies are scanned around two different transitions such that they satisfy a certain configuration [27]. When the detunings of both the lasers is zero from the resonance, we see a peak in transmission at the line center. Let the

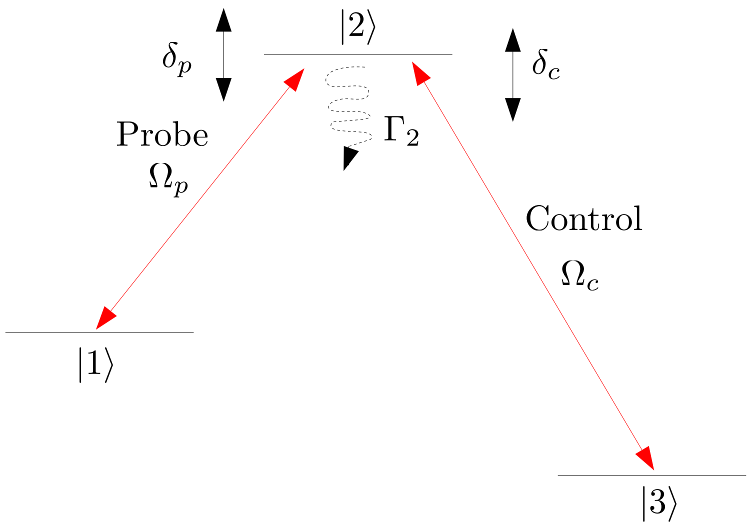

Figure 2.1: A typical EIT process

control field be at a frequency of ω_c, detuning δ_c and Rabi frequency of Ω_c. Similarly, let the probe field have frequency of ω_p, detuning δ_p and Rabi frequency of Ω_p. Let level $|i\rangle$ have a decay rate Γ_i. We assume the ground state will have decay rate zero.

The control field dresses the $|2\rangle$ and $|3\rangle$ levels, and creates some new levels $|+\rangle$ and $|-\rangle$ [28]. These states $|+\rangle$ and $|-\rangle$ are called Autler-Townes Doublets. Now, let us look at EIT mathematically, using all the tools we have developed upto this point. Let the probe and control fields be given by

$$\begin{aligned} \mathcal{E}_p(t) &= \mathcal{E}_{0,p} \cos(\omega_p t)\, \hat{\boldsymbol{\epsilon}}_{\boldsymbol{p}} \\ \mathcal{E}_c(t) &= \mathcal{E}_{0,c} \cos(\omega_c t)\, \hat{\boldsymbol{\epsilon}}_{\boldsymbol{c}} \end{aligned} \tag{2.40}$$

The total Hamiltonian in the RWA for three-level Λ-type system is given by

$$\mathcal{H} = \frac{\hbar}{2} \begin{bmatrix} 0 & \Omega_p & 0 \\ \Omega_p^* & 2\delta_p & \Omega_c^* \\ 0 & \Omega_c & 2(\delta_p - \delta_c) \end{bmatrix} \tag{2.41}$$

where $\Omega_p = -\mathcal{E}_{0,p} \langle 1 | e\mathbf{r} \cdot \hat{\epsilon}_p | 2 \rangle / \hbar$, $\Omega_c = -\varepsilon_{0,c} \langle 3 | e\mathbf{r}.\hat{\epsilon_c} | 2 \rangle / \hbar$. For both the frequencies on resonance, we can define the "mixing angles" θ and ϕ as

$$\begin{aligned} \tan\theta &= \frac{\Omega_p}{\Omega_c} \\ \tan 2\phi &= \frac{\sqrt{|\Omega_p|^2 + |\Omega_c|^2}}{\delta} \end{aligned} \tag{2.42}$$

We solve the equation $H|i\rangle = \lambda |i\rangle$ for probe at a detuning δ and $\delta_p = \delta_c$ and get the following eigenvalues of the Hamiltonian

$$\begin{aligned} \lambda_0 &= 0 \\ \lambda_\pm &= \frac{\hbar}{2}\left[\delta \pm \sqrt{\delta^2 + |\Omega_p|^2 + |\Omega_c|^2}\right] \end{aligned} \tag{2.43}$$

The corresponding eigenstates in terms of the atomic state $|i\rangle$ can be written as

$$\begin{aligned} |0\rangle &= \cos\theta|1\rangle - \sin\theta|3\rangle \\ |+\rangle &= \sin\theta\sin\phi|1\rangle + \cos\phi|2\rangle + \cos\theta\sin\phi|3\rangle \\ |-\rangle &= \sin\theta\cos\phi|1\rangle - \sin\phi|2\rangle + \cos\theta\cos\phi|3\rangle \end{aligned} \tag{2.44}$$

Notice that there are no terms involving $|2\rangle$ in the expression of $|0\rangle$. This is called a dark state as there cannot be a transition to $|2\rangle$ when this state is formed and consequently no decay by spontaneous emission. For a weak probe, we can do the approximation,

$$\Omega_p \ll \Omega_c \Rightarrow \frac{\Omega_p}{\Omega_c} \ll 1 \Rightarrow \tan\theta \ll 1 \Rightarrow \sin\theta \to 0, \cos\theta \to 1 \tag{2.45}$$

Now, $|0\rangle = |1\rangle$ and $\tan 2\phi \to \infty \Rightarrow \phi \to \pi/4$. Then the dressed states are given by

$$\begin{aligned} |+\rangle &= \frac{1}{\sqrt{2}}(|3\rangle + |2\rangle) \\ |-\rangle &= \frac{1}{\sqrt{2}}(|3\rangle - |2\rangle) \end{aligned} \tag{2.46}$$

From Eqn (2.11), we can calculate the susceptibility of the medium in terms of the

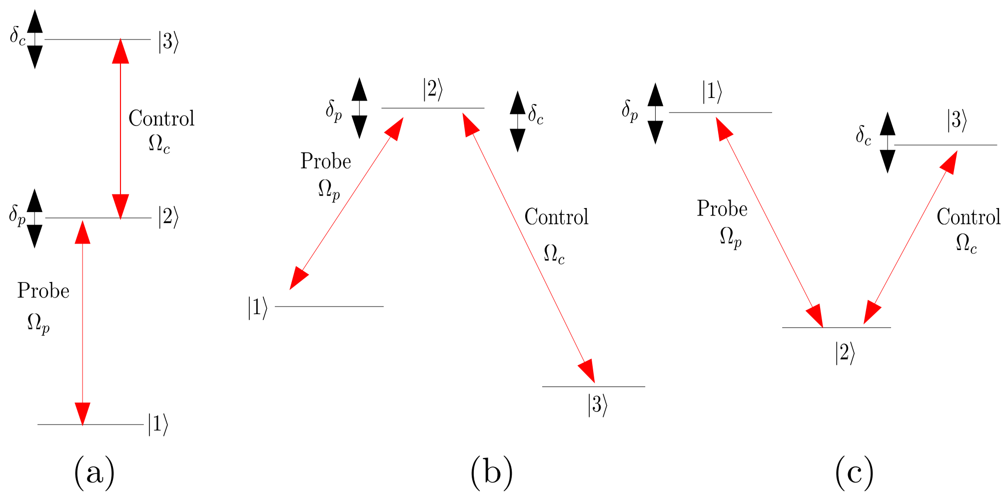

Figure 2.2: a) Ladder, b) lambda and c) vee configurations

density matrix ρ_{12} and show that the medium is transparent for $\delta_p = \delta_c = 0$. The imaginary part of the susceptibility, $\mathrm{Im}(\chi)$ gives the absorption of the medium and at zero detuning for both probe and control, we get a dip in the absorption. The real part of the susceptibility, $\mathrm{Re}(\chi)$ gives the dispersion of the medium. Depending on the slope of the dispersion curve at zero detuning, we can obtain slow or fast light from EIT medium, which lead to a whole range of new experiments. I shall not, however, elaborate on this. Let us now very briefly derive the EIT parameters, that is, the density matrices corresponding to the EIT transition for Λ, Ξ and Vee systems. We are particularly interested in the Ladder type EIT to a Rydberg State, which is called the Rydberg EIT.

Lambda system EIT

Here the relaxation matrix is given by

$$\Gamma = \begin{bmatrix} \gamma & 0 & 0 \\ 0 & \gamma + \Gamma_2 & 0 \\ 0 & 0 & \gamma \end{bmatrix} \tag{2.47}$$

Ground states get repopulated due to spontaneous decay from $|2\rangle$ as well as due to transit relaxation. Assuming atomic polarization will get completely destroyed after wall collisions, atoms will re-enter the beam with populations in the ground states only. So, repopulation matrix takes the form

$$\Lambda = \frac{\gamma + \Gamma_2 \rho_{22}}{2} \begin{bmatrix} 1 & 0 & 0 \\ 0 & 0 & 0 \\ 0 & 0 & 1 \end{bmatrix} \tag{2.48}$$

Then the Bloch Equations become

$$\begin{aligned}
\dot{\rho}_{11} &= -\gamma\rho_{11} + \frac{\gamma}{2} + \frac{\Gamma_2}{2}\rho_{22} + \frac{\mathrm{i}}{2}\left(\Omega_p^*\rho_{12} - \Omega_p\rho_{21}\right) \\
\dot{\rho}_{22} &= -\left(\gamma + \Gamma_2\right)\rho_{22} + \frac{\mathrm{i}}{2}\left(\Omega_p\rho_{21} - \Omega_p^*\rho_{12}\right) + \frac{\mathrm{i}}{2}\left(\Omega_c\rho_{23} - \Omega_c^*\rho_{32}\right) \\
\dot{\rho}_{33} &= -\gamma\rho_{33} + \frac{\gamma}{2} + \frac{\Gamma_2}{2}\rho_{22} + \frac{\mathrm{i}}{2}\left(\Omega_c^*\rho_{32} - \Omega_c\rho_{23}\right) \\
\dot{\rho}_{12} &= \dot{\rho}_{21}^* = \left(-\gamma - \frac{\Gamma_2}{2} + \mathrm{i}\delta_p\right)\rho_{12} + \frac{\mathrm{i}}{2}\Omega_p\left(\rho_{11} - \rho_{22}\right) + \frac{\mathrm{i}}{2}\Omega_c\rho_{13} \\
\dot{\rho}_{13} &= \dot{\rho}_{31}^* = \left(-\gamma + \mathrm{i}\left(\delta_p - \delta_c\right)\right)\rho_{13} + \frac{\mathrm{i}}{2}\left(\Omega_c^*\rho_{12} - \Omega_p\rho_{23}\right) \\
\dot{\rho}_{23} &= \dot{\rho}_{32}^* = \left(-\gamma - \frac{\Gamma_2}{2} - \mathrm{i}\delta_c\right)\rho_{23} + \frac{\mathrm{i}}{2}\Omega_c^*\left(\rho_{22} - \rho_{33}\right) - \frac{\mathrm{i}}{2}\Omega_p^*\rho_{13}
\end{aligned} \tag{2.49}$$

From Eqn (2.11), we can calculate the susceptibility of the medium in terms of the density matrix ρ_{12} and show that the medium is transparent for $\delta_p = \delta_c = 0$. For a non zero probe detuning, an EIT is usually formed by the probe Raman level and the control in resonance with the Raman level and the second excited state. This has been used in our experiment as well, while setting AOM shift values. The density matrix corresponding to the ground and doubly excited state is given by

$$\rho_{12} = \frac{i\Omega_p/2}{\left(\frac{\Gamma_2}{2} - i\delta_p\right) + \frac{i\left|\Omega_c\right|^2/4}{\left(\delta_p - \delta_c\right)}} \tag{2.50}$$

Now, before we move on to the ladder system, let us talk about Vee system EIT.

Vee system EIT

Here, $|2\rangle$ is the common ground state and $|1\rangle$ and $|3\rangle$ are the excited states. The total Hamiltonian in RWA is given by

$$\mathcal{H} = \frac{\hbar}{2}\begin{bmatrix} 2\delta_p & \Omega_p^* & 0 \\ \Omega_p & 0 & \Omega_c \\ 0 & \Omega_c^* & 2\delta_c \end{bmatrix} \tag{2.51}$$

The relaxation matrix is given by

$$\Gamma = \begin{bmatrix} \gamma+\Gamma_1 & 0 & 0 \\ 0 & \gamma & 0 \\ 0 & 0 & \gamma+\Gamma_3 \end{bmatrix} \tag{2.52}$$

Repopulation matrix is given by

$$\Lambda = \begin{bmatrix} 0 & 0 & 0 \\ 0 & \gamma+\Gamma_1\rho_{11}+\Gamma_3\rho_{33} & 0 \\ 0 & 0 & 0 \end{bmatrix} \tag{2.53}$$

After solving the Bloch Equations we get

$$\rho_{33} = \frac{\dfrac{|\Omega_c|^2}{\Gamma_3^2}}{1+\dfrac{2\,|\Omega_c|^2}{\Gamma_3^2}+\dfrac{4\delta_c^2}{\Gamma_3^2}} \tag{2.54}$$

However, the population in state $|1\rangle$ can be approximated to zero. So, in V system, we have, $\rho_{11} \simeq 0, \rho_{22} \neq 0, \rho_{33} \neq 0$ such that $\rho_{11}+\rho_{22}+\rho_{33}=1$. The steady state solution for ρ_{21} (with $\gamma = 0$) is

$$\rho_{21} = \frac{i\Omega_p\left[\left(\Gamma_3^2+4\delta_c^2+|\Omega_c|^2\right)-\dfrac{|\Omega_c|^2\left(\dfrac{\Gamma_3}{2}-i\delta_c\right)}{\left(\dfrac{\Gamma_1+\Gamma_3}{2}+i\left(\delta_c-\delta_p\right)\right)}\right]}{2\left(\Gamma_3^2+4\delta_c^2+2\,|\Omega_c|^2\right)\left[\dfrac{\Gamma_1}{2}-i\delta_p+\dfrac{|\Omega_c|^2/4}{\left(\dfrac{\Gamma_1+\Gamma_3}{2}+i\left(\delta_c-\delta_p\right)\right)}\right]} \tag{2.55}$$

Now we move on to the Ladder system. Before we do, let us have a look at the ^{87}Rb energy levels (Fig. 2.3).

Ladder system EIT

Let us start as before by writing down the total Hamiltonian in the RWA

$$\mathcal{H} = \frac{\hbar}{2}\begin{bmatrix} 0 & \Omega_p & 0 \\ \Omega_p^* & 2\delta_p & \Omega_c \\ 0 & \Omega_c^* & 2\left(\delta_p+\delta_c\right) \end{bmatrix} \tag{2.56}$$

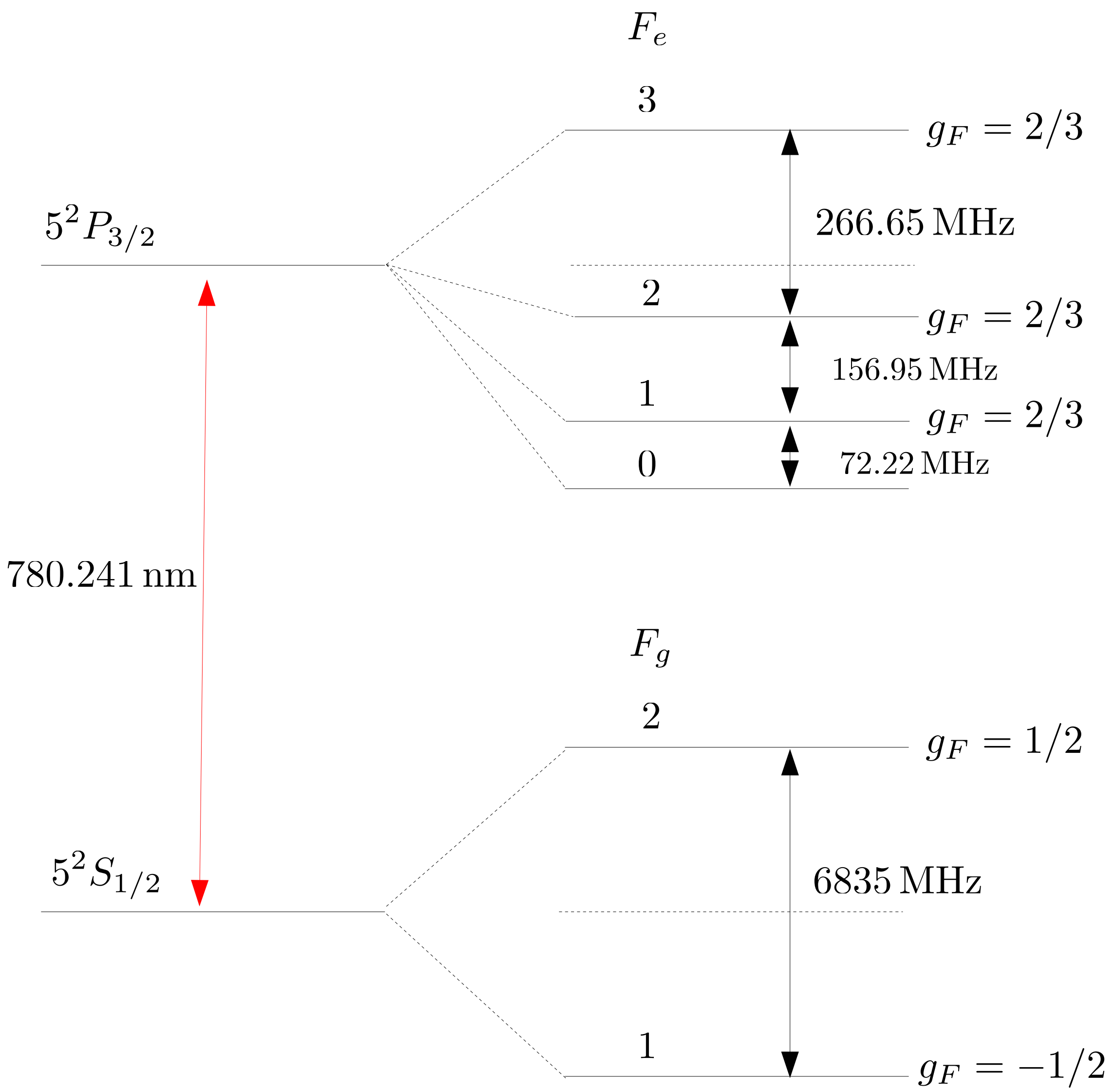

Figure 2.3: ^{87}Rb energy levels

The relaxation matrix is of the form

$$\Gamma = \begin{bmatrix} \gamma & 0 & 0 \\ 0 & \gamma + \Gamma_2 & 0 \\ 0 & 0 & \gamma + \Gamma_3 \end{bmatrix} \tag{2.57}$$

Ground state $|1\rangle$ and first excited state $|2\rangle$ will get repopulated due to spontaneous decay from state $|2\rangle$ and $|3\rangle$ respectively. Transit relaxation rate γ will repopulate the ground states $|1\rangle$ only. So, the repopulation matrix can be written as

$$\Lambda = \begin{bmatrix} \gamma + \Gamma_2\rho_{22} & 0 & 0 \\ 0 & \Gamma_3\rho_{33} & 0 \\ 0 & 0 & 0 \end{bmatrix} \tag{2.58}$$

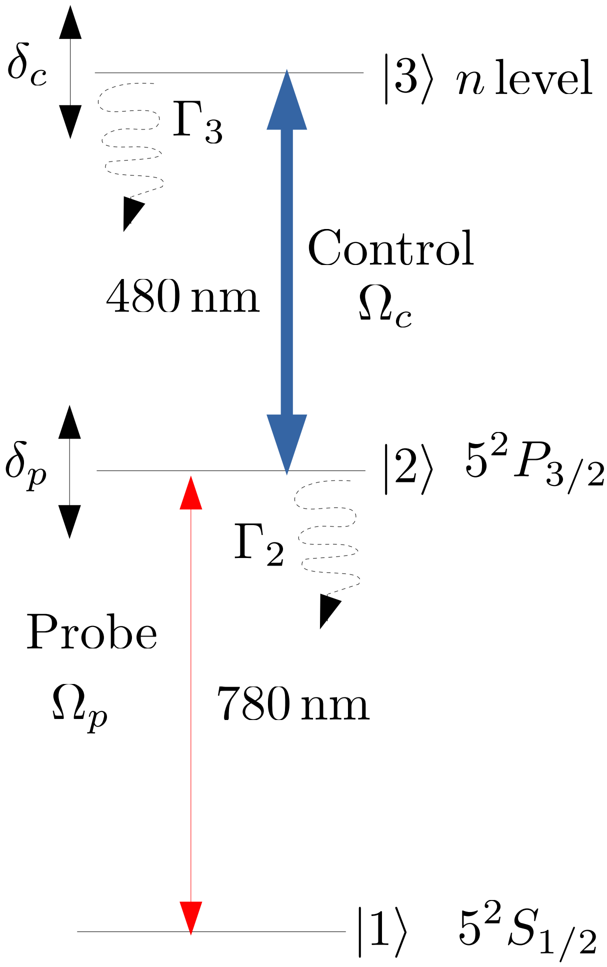

Figure 2.4: Rydberg EIT—a ladder type EIT

Now, the density matrix equations are

$$
\begin{aligned}
\dot{\rho}_{11} &= -\gamma\rho_{11} + \gamma + \Gamma_2\rho_{22} + \frac{1}{2}\left(\Omega_p^*\rho_{12} - \Omega_p\rho_{21}\right) \\
\dot{\rho}_{22} &= -\left(\gamma + \Gamma_2\right)\rho_{22} + \Gamma_3\rho_{33} + \frac{\mathrm{i}}{2}\left(\Omega_p\rho_{21} - \Omega_p^*\rho_{12}\right) + \frac{\mathrm{i}}{2}\left(\Omega_c^*\rho_{23} - \Omega_c\rho_{32}\right) \\
\dot{\rho}_{33} &= -\left(\gamma + \Gamma_3\right)\rho_{33} + \frac{\mathrm{i}}{2}\left(\Omega_c\rho_{32} - \Omega_c^*\rho_{23}\right) \\
\dot{\rho}_{12} = \dot{\rho}_{21}^* &= \left(-\gamma - \frac{\Gamma_2}{2} + \mathrm{i}\delta_p\right)\rho_{12} + \frac{\mathrm{i}}{2}\Omega_p\left(\rho_{11} - \rho_{22}\right) + \frac{\mathrm{i}}{2}\Omega_c^*\rho_{13} \\
\dot{\rho}_{13} = \dot{\rho}_{31}^* &= \left(-\gamma - \frac{\Gamma_3}{2} + \mathrm{i}\left(\delta_p + \delta_c\right)\right)\rho_{13} + \frac{\mathrm{i}}{2}\left(\Omega_c\rho_{12} - \Omega_p\rho_{23}\right) \\
\dot{\rho}_{23} = \dot{\rho}_{32}^* &= \left(-\gamma - \frac{\Gamma_2 + \Gamma_3}{2} + \mathrm{i}\delta_c\right)\rho_{23} + \frac{\mathrm{i}}{2}\Omega_c\left(\rho_{22} - \rho_{33}\right) - \frac{\mathrm{i}}{2}\Omega_p^*\rho_{13}
\end{aligned}
\tag{2.59}
$$

We find the steady state solution for ρ_{12} as

$$\rho_{12} = \frac{i\Omega_p/2}{\left(\frac{\Gamma_2}{2} - i\delta_p\right) + \frac{|\Omega_c|^2/4}{\left(\frac{\Gamma_3}{2} - i\left(\delta_p + \delta_c\right)\right)}} \tag{2.60}$$

Taking into account the velocity of the atoms, we get the expression for susceptibility of the medium as

$$\begin{aligned}\chi(v)\mathrm{d}v = -i\frac{3\lambda_{\mathrm{p}}^2}{4\pi}\gamma_2 N(v)\mathrm{d}v\,[\gamma_2 - i\left(\Delta_p - \boldsymbol{k}_{\mathrm{p}}\cdot\boldsymbol{v}\right) + \\ \frac{(\Omega_{\mathrm{c}}/2)^2}{\gamma_3 - i\left(\Delta_p + \Delta_{\mathrm{c}} - (\boldsymbol{k}_{\mathrm{p}} + \boldsymbol{k}_{\mathrm{c}})\cdot\boldsymbol{v}\right)}]^{-1}\end{aligned} \tag{2.61}$$

One can find that for zero detuning of the probe and control, one gets a dip in the Im(χ), which gives the absorption. As shown in Fig. (2.4), we are performing experiments with ^{87} Rb, and the corresponding transitions for the Rydberg EIT are shown, along with rough values of the frequencies of the transitions. Depending on the n level, we get various interesting features, which shall be elaborated in the Results and Analysis Section.

3

Squeezed states from the Rydberg blockade

In this chapter, a brief theory of squeezed states of light will be introduced. I shall start by quantising the electromagnetic field and expressing it as a multi mode quantum harmonic oscillator. Then I go on to describe coherent states, Fock states and squeezed states. Then we briefly describe the theory and the working principles of the balanced homodyne detection scheme for detecting squeezing in a certain quadrature. I end the chapter with a short review on nonlinearities arising from the Rydberg Blockade. I also discuss how these nonlinearities can be exploited for quantum optics and quantum information, and how the Rydberg blockade can be a probable source for squeezed light.

3.1 Quantising the electromagnetic field in free space

Consider an EM wave in a resonating cavity of length L and volume V. Let the electric field associated with it oscillate in the x direction. The normal modes of the cavity can then be expressed as

$$E_x(z,t) = \sum_s A_s q_s(t) \sin(k_s z)\hat{x} \tag{3.1}$$

where s is a positive integer. Here, $q_s(t)$, $k_s = s(\pi/L)$, $\nu_s = s(c/2L)$ are the normal mode amplitude, wave-vectors and eigen-frequencies of the electric field. $A_s = \sqrt{\dfrac{2\nu_s^2 m_s}{\epsilon_0 V}}$ and m_s is a constant with dimension of mass. These modes are the Fourier expansion of the normal mode frequencies for this cavity, and are essentially the solutions of the Helmholtz equation $((\nabla)^2 + k^2)A = 0)$ with the boundary conditions- E(z=0,t)=E(z=L,t)=0. Now, using Maxwell's equations,

$$\nabla \times \vec{H} = \epsilon_0 \frac{\partial \vec{E}}{\partial t} \tag{3.2}$$

We find the magnetic field as

$$H_y(z,t) = \sum_s \epsilon_0 A_s \frac{q_s\dot{(t)}}{k_s} \cos(k_s z)\hat{y} \tag{3.3}$$

The classical Hamiltonian is given by

$$H = \frac{1}{2}\int_V [\epsilon_0 E_x^2 + \mu_0 H_y^2] dV \tag{3.4}$$

Naturally, the integration is over the entire cavity volume. Now we need to simplify this and quantise the field. Quantisation conditions, in general, are usually invoked from the generalised position and momentum commutation relation. Simplification gives the Hamiltonian as

$$H = \frac{1}{2}\sum_s [m_s v_s^2 q_s^2 + \frac{p_s^2}{m_s}] \tag{3.5}$$

where p_s and q_s are the canonical momentum and postion of the s^{th} mode of the field. Now we quantise the field by identifying $\hat{p_s}$ and $\hat{q_s}$ as operators and they follow the commutation relations

$$[\hat{q_s}, \hat{q_{s'}}] = [\hat{p_s}, \hat{p_{s'}}] = 0 \tag{3.6}$$

$$[\hat{q_s}, \hat{p_{s'}}] = \mathrm{i}\hbar\delta_{s,s'} \tag{3.7}$$

Define ladder operator a and $a^\dagger$ as

$$\hat{a_s} = \frac{1}{\sqrt{2\hbar m_s \nu_s}}[m_s \nu_s \hat{q_s} + \mathrm{i}\hat{p_s}]e^{\mathrm{i}\nu_s t} \tag{3.8}$$

$$\hat{a_s}^\dagger = \frac{1}{\sqrt{2\hbar m_s \nu_s}}[m_s \nu_s \hat{q_s} - \mathrm{i}\hat{p_s}]e^{-\mathrm{i}\nu_s t} \tag{3.9}$$

They have the commutation relations

$$[\hat{a_s}, \hat{a_{s'}}] = [\hat{a_s}^\dagger, \hat{a_{s'}}^+] = 0 \tag{3.10}$$

$$[\hat{a_s}, \hat{a_{s'}}^+] = \delta_{s,s'} \tag{3.11}$$

Now, in terms of these ladder operators, the Hamiltonian undergoes a transformation from one set of coordinates to another, and we can express the Hamiltonian as

$$H = \sum_s h\nu_s \left[\hat{a_s}^\dagger \hat{a_s} + \frac{1}{2}\right] \tag{3.12}$$

Now we proceed to actually write down the quantised $\vec{E}$ and $\vec{H}$ fields. For that, we first find the conjugate position and momentum in terms of the ladder operators. Our fields have already been expressed in terms of these. We want to find the solutions of the wave equation in free-space and we want to express our wave as a travelling wave. A direct simplification of the above equations will give us standing wave solutions (in terms of *sine* and *cosine* of the wave number k_j for a field summed over the modes represented by j). We break these down in terms of exponentials. In terms of ladder operators, the $\vec{E}$ and $\vec{H}$ fields can be expressed as

$$E_x(z,t) = \sum_j C_j[\hat{a_j}e^{-\mathrm{i}\nu_j t} + \hat{a_j}^+ e^{\mathrm{i}\nu_j t}]\left(\frac{e^{\mathrm{i}k_j z} - e^{-\mathrm{i}k_j z}}{2\mathrm{i}}\right) \tag{3.13}$$

$$H_y(z,t) = \sum_j \mathrm{i}\epsilon_0 c C_j[\hat{a_j}^+ e^{\mathrm{i}\nu_j t} - \hat{a_j}e^{-\mathrm{i}\nu_j t}]\left(\frac{e^{\mathrm{i}k_j z} + e^{-\mathrm{i}k_j z}}{2}\right) \tag{3.14}$$

where $C_j = \sqrt{\dfrac{h\nu_j}{\epsilon_0 V}} = \sqrt{\dfrac{h}{2m_j\nu_j A_j}}$ A simple expansion of the expression for the fields will show that they contain a term with a positive phase velocity, something we can see in experiments, and a term with a negative phase velocity, which is unrealistic. We restrict ourselves to the realistic solutions.We also generalise our expression to any travelling EM wave. For that, we replace z by r and k_j by k, although we still sum over the modes represented by j. We denote the $\hat{a}^\dagger$ terms by a Hermitian Conjugate (H.c). Then the final expression for our quantised fields are-

$$E_x(z,t) = -\frac{\mathrm{i}}{2}\sum_j C_j[\hat{a_j}e^{-\mathrm{i}\nu_j t + \mathrm{i}\vec{k}.\vec{r}} + H.c]\hat{q_k} \tag{3.15}$$

$$H_y(z,t) = -\frac{\mathrm{i}}{2}\sum_j \mathrm{i}\epsilon c C_j[\hat{a_j}e^{-\mathrm{i}\nu_j t + \mathrm{i}\vec{k}.\vec{r}} - H.c]\hat{p_k} \tag{3.16}$$

where $\hat{q_k}$ is the unit vector for alignment of the polarisation vector for the $\vec{E}$-field, and the polarisation vector for the $\vec{H}$-field is along unit vector $\hat{p_k} = \vec{k} \times \hat{q_k}$.

We define the number operator $\hat{n_k}$ as $\mathbf{\hat{n_k}} = \mathbf{\hat{a_k}}^{+}\mathbf{\hat{a_k}}$.The expectation value of $\hat{n_k}$ is the average number of photons in the k^{th} mode. This is the quantum optics analogue of intensity. The expression for the Hamiltonian (eqn. 2.12) physically means that a mutlimode EM field can be represented as an infinite number of uncoupled quantum harmonic oscillators in a Hilbert space, each with some number of photons, corresponding to energy $\hbar\omega(n+\frac{1}{2})$ for a mode with n photons. This brings us to the idea of a photon number state, or a Fock state, which we shall formally introduce in the next section.

3.2 Fock states, coherent states and uncertainty of conjugate variables

The ladder operators enable us to define states with increasing energy levels given by the number of photons in a certain state. As already mentioned, these states are called photon **number states**, or Fock states. Let us denote a single mode number state by $|n\rangle$. These are, by definition, eigenstates of the Hamiltonian and we can write

$$\hat{H}\,|n\rangle = E\,|n\rangle = \left(n+\frac{1}{2}\right)\hbar\omega\,|n\rangle \tag{3.17}$$

where $\langle n|n'\rangle = \delta_{nn'}$. We define the **creation operator**, or rather, name one of the ladder operators the creation operator, with the property

$$\hat{a}^{\dagger}\,|n\rangle = \sqrt{n+1}\,|n+1\rangle \tag{3.18}$$

The **annihilation operator** is likewise defined as

$$\hat{a}\,|n\rangle = \sqrt{n}\,|n-1\rangle \tag{3.19}$$

The ground state $|0\rangle$ is the state where the system hasn't been excited by any quanta of light, or rather, a state which contains no photons. This is termed the **vacuum state** and any number state $|n\rangle$ can be built up from the vacuum state by repeated appliction of the creation operator, so that we have

$$|n\rangle = \frac{1}{\sqrt{n!}}(\hat{a}^{\dagger})^{n}\,|0\rangle \tag{3.20}$$

We define the vacuum state in such a way such that $\hat{a}\,|0\rangle = 0$. As is understood, contrary to classical field theory, there exists a vacuum fluctuation of the quantised EM field. The average value of this fluctuation is $\frac{1}{2}\hbar\omega$.

Define a **coherent state** as an eigenstate of the annihilation operator such that $\hat{a}\,|\alpha\rangle = \alpha\,|\alpha\rangle$. Of course, this can be expressed in terms of the number state as $|\alpha\rangle = \sum_n C_n\,|n\rangle$ where $C_n = \langle n|\alpha\rangle$. Now,

$$\hat{a}\,|\alpha\rangle = \sum_n \alpha C_n\,|n\rangle = \sum_n C_n\sqrt{n}\,|n-1\rangle \tag{3.21}$$

Equating the terms for the same state, we get $C_n = \frac{\alpha^n}{\sqrt{n!}} C_0$ and so we can write the coherent state in terms of the number state as

$$|\alpha\rangle = \sum_n \frac{\alpha^n}{\sqrt{n!}} C_0 |n\rangle \tag{3.22}$$

We normalise this and find $|C_0| = e^{-|\alpha|^2/2}$. Then,

$$|\alpha\rangle = e^{-|\alpha|^2/2} \sum_n \frac{\alpha^n}{\sqrt{n!}} |n\rangle \tag{3.23}$$

In terms of the vacuum state, the coherent state is

$$|\alpha\rangle = e^{-|\alpha|^2/2} \sum_n \frac{(\alpha \hat{a}^\dagger)^n}{n!} |0\rangle = e^{-|\alpha|^2/2} e^{\alpha \hat{a}^\dagger} |0\rangle \tag{3.24}$$

Now, $e^{-\alpha^* \hat{a}} |0\rangle = |0\rangle$ So, the Coherent state can be shown to be a **displaced vacuum state**. Apply the Baker-Hausdorff formula with A and B operators as $e^{\alpha \hat{a}^\dagger}$ and $e^{-\alpha^* \hat{a}}$ to obtain

$$|\alpha\rangle = \hat{D}(\alpha) |0\rangle = e^{\alpha \hat{a}^\dagger - -\alpha^* \hat{a}} |0\rangle \tag{3.25}$$

where $\hat{D}(\alpha)$ is the displacement operator. Now, another important observation regarding the Coherent state is its probability distribution, that is, the probability of finding n photons in the state $|\alpha\rangle$. This is given by

$$P(n) = |\langle n|\alpha\rangle|^2 = e^{-|\alpha|^2} \frac{(|\alpha|^2)^n}{n!} = e^{-\langle n\rangle} \frac{\langle n\rangle^n}{n!} \tag{3.26}$$

So, this probability distribution is Poisson. Most lasers produce coherent states and the photons follow a Poisson distribution. This sort of light is called Poissonian light. There are other non classical states of light which are sub-poissonian or super-poissonian in nature. One such very important form of light is a squeezed state, which is a sub-poissonian state of light, which shall be described in more details in the next section.

At this point, we must also mention **shot noise**. To speak very simply, shot noise is the noise in our photodetection arising from the Poissonian nature of our light. It is just the uncertainty in the exact value of our classical intensity from the photodetector, which is after all a classical device, due to the quantum nature of light [7]. More on analysis of shot noise shall be discussed in the following sections and chapters of this thesis. Before we go on to Squeezed states, let us say a few more things about Coherent States and uncertainty of our observables in a quantum measurement.
Solving the Schrödinger equation for a single mode field in the Coherent State representation, we get the wave function

$$\psi_0 = (\frac{\nu}{\pi\hbar})^{1/4} e^{-\nu q^2/2\hbar} \tag{3.27}$$

which represents a Gaussian Wave Packet. Now let us calculate the uncertainties in the observables p and q. With respect to this wave function, the uncertainties are given by

$$\Delta q = \sqrt{\langle q^2\rangle - \langle q\rangle^2} = \sqrt{\frac{\hbar}{\nu}\left(n + \frac{1}{2}\right)} \tag{3.28}$$

$$\Delta p = \sqrt{\langle p^2\rangle - \langle p\rangle^2} = \sqrt{\hbar\nu\left(n + \frac{1}{2}\right)} \tag{3.29}$$

So the uncertainty product of these variables is

$$\Delta p \Delta q = \hbar(n + \frac{1}{2}) \tag{3.30}$$

The ground state uncertainty is $\frac{\hbar}{2}$ while the first excited state uncertainty is $\frac{3\hbar}{2}$. For a displacement operator acting on a vacuum state, the wave function can be found by a coordinate transformation from q to some $(q - q_0)$. The coherent state remains a quantum harmonic oscillator just translating in the Hilbert space.

3.3 Squeezed states and the balanced homodyne detection scheme

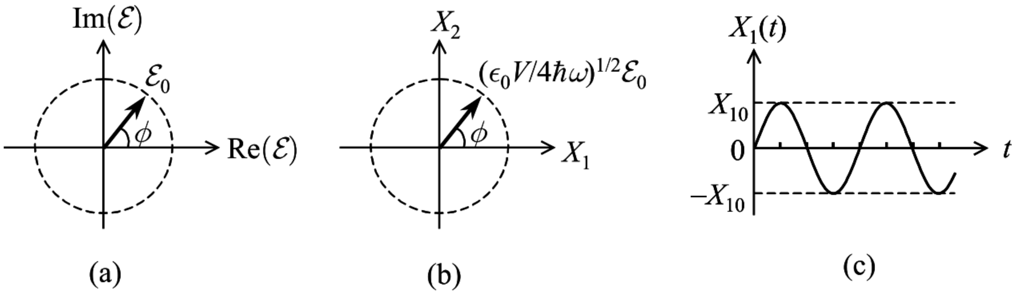

Figure 3.1: a) Phasor diagram for a classical wave of phase ϕ and amplitude E_0; b) phasor diagram in quadrature units with each axes being a quadrature; c) time dependence of the X_1 field quadrature.

Let us start by a brief treatment of phasor diagrams and field quadratures. We know that any classical field can be expressed as a phasor $\vec{E} = E_0 e^{i\phi}$. Likewise, in quantum optics, it is convenient to work with quantities that are dimensionless and we would want to express any state as a phasor like this, with the two axes called **field quadratures**. For a classical travelling electric field, the quadratures, for example, can be defined as

$$X_1(t) = \left(\frac{\epsilon_0 V}{4\hbar\omega}\right)^{1/2} E_0 \sin\omega t \tag{3.31}$$

$$X_2(t) = \left(\frac{\epsilon_0 V}{4\hbar\omega}\right)^{1/2} E_0 \cos\omega t \tag{3.32}$$

Likewise, a coherent state can also be expressed as a phasor with certain quadrature amplitudes. Define α as

$$\alpha = |\alpha|e^{\mathrm{i}\phi} = X_1 + \mathrm{i}X_2 \tag{3.33}$$

The two quadratures have equal uncertainty and are expressed as

$$X_1 = |\alpha| \cos\phi \tag{3.34}$$

$$X_2 = |\alpha| \sin\phi \tag{3.35}$$

$$\Delta X_1 = \Delta X_2 = \frac{1}{2} \tag{3.36}$$

Here,

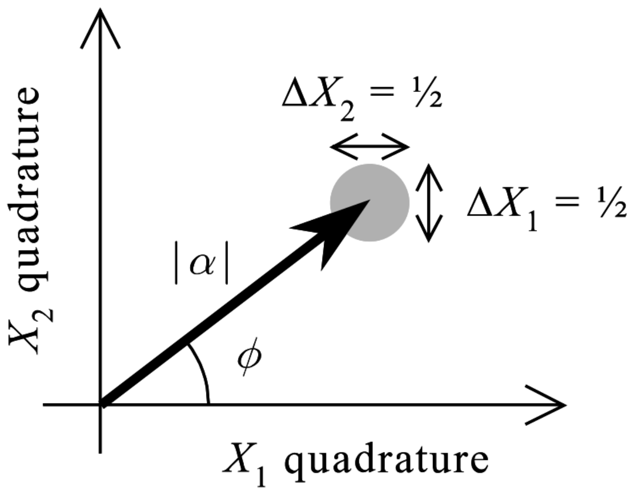

Figure 3.2: Phasor diagram for a coherent state showing the quadrature values.

$$|\alpha| = \sqrt{\frac{\epsilon_0 V}{4\hbar\omega}} E_0 \tag{3.37}$$

In general, we can define quadrature operators as

$$\hat{X}_1 = \frac{\hat{a} + \hat{a}^\dagger}{2} \text{ and } \hat{X}_2 = \frac{\hat{a} - \hat{a}^\dagger}{2i} \tag{3.38}$$

These operators, when operated on a certain “coherent-like” state, or, a state, which can be expanded in a Fock basis, gives the component of the state along a certain quadrature. Essentially, it collapses the state from a Hilbert space to a 2D space called the “quadrature phase space” and then the expectation value of this operator gives the component of the quantum field of this state along that quadrature. We can also write a **number-phase uncertainty** as

$$\Delta n \Delta \phi \geqslant 1/2 \tag{3.39}$$

This shows that it is not possible to know the photon number (i.e. the amplitude) and the phase of a wave with perfect precision at the same time.

Squeezed states are states with unequal uncertainties in the two quadratures. That is, one quadrature can be measured very accurately while the other quadrature cannot. And by accurately, I mean the uncertainty is lesser than the standard quantum limit. That is, for a shot noise limited system, the uncertainty (or the variance) is less than the level of shot noise at that quadrature. A **shot noise limited** system is a system where the classical noise is minimised as much as possible and the system is able to see quantum noise. This means that considering all other forms of noise apart from shot noise as N (say), the total noise TN is greater than or equal to 2N. So, the dominant form of noise will be shot noise. A shot noise limited system is necessary to detect any form of non-classical light, especially squeezed light, as we want to measure how much the squeezing has been with reference to the standard shot noise at a certain intensity of our field. This is usually detected by measuring the variance of the signal for enoughly small bins in time.

For a coherent state, the variance is equal for all bins. Depending on what phenomenon we are obtaining the squeezing from, the timescale of the bin will be set. For our case, as in for atomic transitions, we would want at least a microsecond bin. In a squeezed state, the uncertainty in one quadrature transcends beyond the standard quantum limit while the uncertainty in the other quadrature gets higher. One way in which this can be achieved is to squeeze the uncertainty circle of the vacuum or the coherent state into an ellipse of the same area. Such states are called quadrature-squeezed states. Figures 3.3(b) and 3.3(c) illustrate two other forms of squeezed light in which the uncertainty circle of the coherent state has been squeezed into an ellipse of the same area. In (b) the major axis of the ellipse has been aligned with the phasor of the coherent state, so that the phase uncertainty is smaller than that in the original coherent state, while in (c) the minor axis has been aligned in order to reduce the amplitude uncertainty. The two states are therefore called phase-squeezed light and amplitude squeezed light, respectively. Squeezed states are used extensively in various kinds of precision measurements. For example, the LIGO interfereometer uses squeezed vacuum for all its meausurements to get better accuracy. [29] [30]

Mathematically, the squeezing operator for a single mode EM field is given by

$$\hat{S}(z) = \exp\left(\frac{1}{2}\left(z^{*}\hat{a}^{2} - z\hat{a}^{\dagger 2}\right)\right), \quad z = re^{i\theta} \tag{3.40}$$

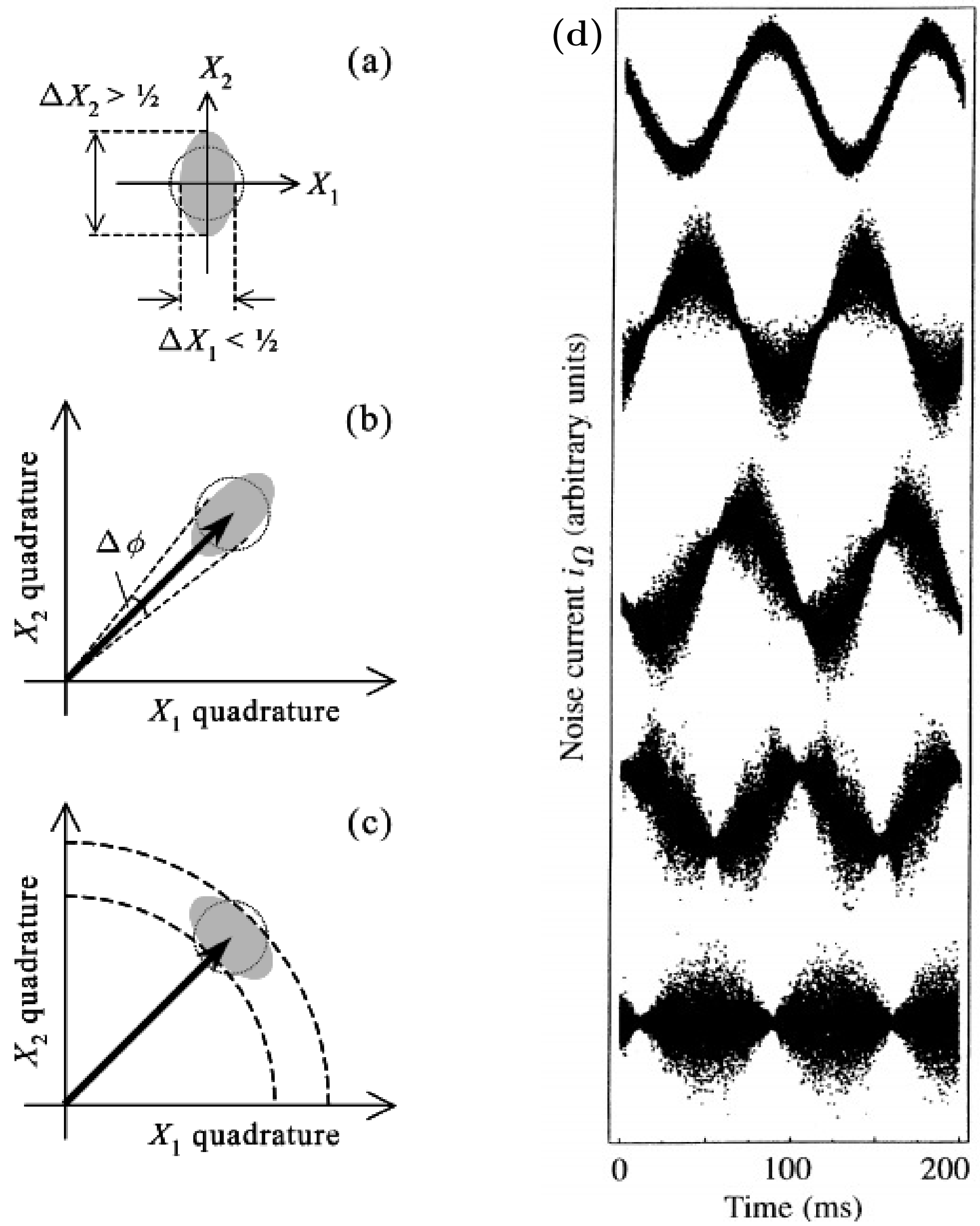

Figure 3.3: Darker circle shows the squeezed state uncertainty; a) quadrature values of a squeezed state-squeezed vacuum in this case; b) phase-squeezed light; c) amplitude-squeezed light; d) output current with time of the balanced homodyne detector circuit.

where $\hat{S}(z)$ is a unitary operator and follows $S(\zeta)S^{\dagger}(\zeta) = S^{\dagger}(\zeta)S(\zeta) = \hat{\mathbf{1}}$. r is the magnitude of the phasor in the quadrature phase space.The action of the squeezing operator on creation and annihilation operators produce

$$\hat{S}^{\dagger}(z)\hat{a}\hat{S}(z) = \hat{a}\cosh r - e^{i\theta}\hat{a}^{\dagger}\sinh r \quad \text{and} \quad \hat{S}^{\dagger}(z)\hat{a}^{\dagger}\hat{S}(z) = \hat{a}^{\dagger}\cosh r - e^{-i\theta}\hat{a}\sinh r \quad (3.41)$$

Squeezed states can be detected by a **balanced homodyne detection scheme** (Fig. 3.4). In this kind of detection, denote the field for which squeezing is to be detected as the signal field. This field is made incident on a 50:50 beam splitter along with a local oscillator field. The local oscillator field is usually a field from the same source-the same laser or whatever, which usually has a very large amplitude compared to the signal field and has a pre-determined phase difference with the signal field. The two fields are made to fall on the beamsplitter after traversing more or less the same path length with a very high mode match percentage at the beamsplitter. The local oscillator path has a piezo connected to one of the mirrors which can change the path length and hence the phase. After the beamsplitter, the two fields are made to fall on two photodiodes PD_1 and PD_2. The difference current is measured. As shown in the figure 3.4, the output fields ε_1 and ε_2 are

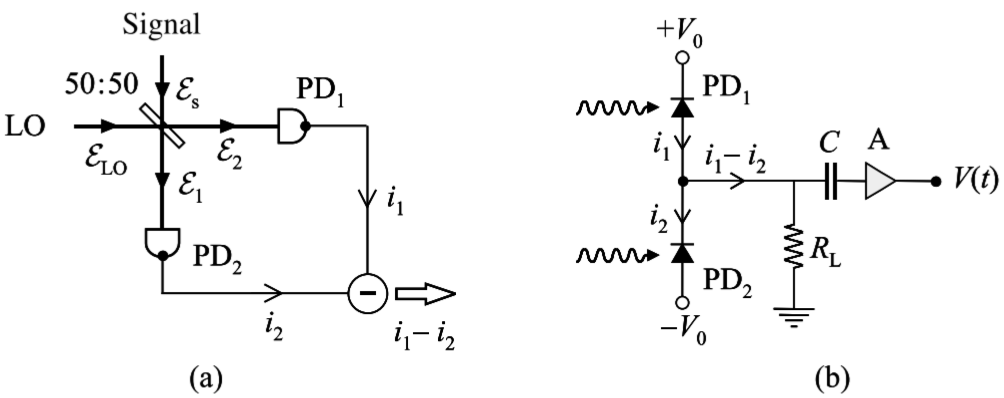

Figure 3.4: a) A schematic of a general homodyne detection setup; b) Typical circuitry of the homodyne photodetector output .

given by

$$\varepsilon_1 = \frac{1}{\sqrt{2}}(\varepsilon_{LO}e^{\mathrm{i}\phi_{LO}} + \varepsilon_s) \tag{3.42}$$

$$\varepsilon_2 = \frac{1}{\sqrt{2}}(\varepsilon_{LO}e^{\mathrm{i}\phi_{LO}} - \varepsilon_s) \tag{3.43}$$

Now we split the field into its two quadrature components.

$$\varepsilon_s = \varepsilon_s^{X_1} + \mathrm{i}\varepsilon_s^{X_2} \tag{3.44}$$

Then, splitting the output fields into their real and imaginary parts in terms of the quadrature fields gives us

$$\varepsilon_1 = \frac{1}{\sqrt{2}}(\varepsilon_{LO}\cos\phi_{LO} + \varepsilon_s^{X_1}) + \mathrm{i}(\varepsilon_{LO}\sin\phi_{LO} + \varepsilon_s^{X_2}) \tag{3.45}$$

$$\varepsilon_2 = \frac{1}{\sqrt{2}}(\varepsilon_{LO}\cos\phi_{LO} - \varepsilon_s^{X_1}) + \mathrm{i}(\varepsilon_{LO}\sin\phi_{LO} - \varepsilon_s^{X_2}) \tag{3.46}$$

Then, the output is proportional to $(i_1 - i_2)$ which are in turn proportional to the field amplitudes $\varepsilon_1\varepsilon_1^*$ and $\varepsilon_2\varepsilon_2^*$. So, we can write

$$\text{Output} \propto 2\varepsilon_{LO}(\cos\phi_{LO}\varepsilon_s^{X_1} + \sin\phi_{LO}\varepsilon_s^{X_2}) \tag{3.47}$$

As is clear from the equation, we are stroboscopically looking at the two field quadratures at different phase values. For certain phase values, the first term vanishes and for certain other phase values, the second term vanishes. At these values, we are essentially looking at the field quadrature amplitudes directly, amplified by the LO field. The LO field does precisely the same, that is, it amplifies the output and increases the value of our signal even for very weak fields.
One can see the how the output looks like in Fig. 3.3(d). This is from a landmark paper [31] in the field of squeezing by *Breitenbach et al* published in *Nature* where squeezing was produced from an Optical Parametric Oscillator for the first time. The first signal is the output from a balanced homodyne detector for a coherent state, the second for a phase squeezed state, the third for squeezing at a certain angle of the phasor not $n\pi/2$ or $n\pi$, the fourth for amplitude squeezing and the fifth for squeezed vacuum. One can clearly see that the variance of the signal at various phase values varies for squeezed light. A more mathematical treatment of variance and characterisation of a balanced homodyne detector, that we developed, shall be given as a support for our data in the "Results and Analysis" section. Figures 3.1, 3.2, 3.3 a), b), c) have been taken from the book "Introduction to Quantum Optics" by Mark Fox.

3.4 The Rydberg blockade

Rydberg atoms have been extensively studied to explore the various effects arising from the large dipole moment between the highly excited electron and the nucleus. One such effect is the presence of the Rydberg Blockade. The advantage of the Rydberg nonlinearity over conventional nonlinear processes such as the Kerr Effect arising from a third-order nonlinearity, is that dipole-dipole interactions are usually long-range and stronger. I have already stated the goals of using Rydberg transitions and the various fundamental ways in which it can be used in the Introduction. Here, I will very briefly note down some of the characteristics of the Rydberg transition. For a more detailed discussion, a very nice review paper on this topic has been published by Firstenberg *et al.* [10]

One of the biggest achievements in exploring Rydberg transitions was to obtain the Rydberg EIT. In 2005, Friedler et al for the first time discussed the idea that one could couple the doubly excited state in a ladder type EIT to highly excited Rydberg states which are metastable [32]. They showed that one could "transfer the strong interactions between Rydberg atoms onto the optical transition and thereby realize a photonic phase gate". The first experimental demonstrations of the Rydberg EIT upto n=124 was done by Mohapatra *et al* in 2007 [14].The first experiments to show the nonlinearities arising from the Rydberg blockade in an ultracold atomic ensemble were performed in 2010 in CS

Adams' group [33]. Recently, the nonlinear nature of the Rydberg Blockade in a thermal vapour cell has also been shown by employing a heterodyne method of detection [12]. The possiblity to create entangled quantum states using the Rydberg blockade has resulted in proposals to use Rydberg atoms as the building blocks of a quantum computer [34], and the first proof-of-principle experiments have already been carried out [35].

We will briefly outline the mathematics behind Rydberg atoms and the Rydberg blockade.

3.4.1 Dipole-dipole and van der Waals interactions

Rydberg atoms are very sensitive to external electric fields, with their polarizability scaling with the principal quantum number like n^7. To analyze the strong interactions in Rydberg atoms, we consider that their electron wave functions don't overlap andd that they are far enough apart. As the Rydberg wave functions decay exponentially at large distances, it is possible to express this in terms of a single quantity, the Le Roy radius R_{LR}, which is given by

$$R_{LR} = 2\left(\sqrt{\langle n_1, l_1 \left| r^2 \right| n_1, l_1\rangle} + \sqrt{\langle n_2, l_2 \left| r^2 \right| n_2, l_2\rangle}\right) \tag{3.48}$$

where $|n_i, l_i\rangle$ refers to the electron eigenstate of the ith atom. Treating the Rydberg electrons as hydrogenic, we obtain for the expectation value

$$\left\langle r^2 \right\rangle = \frac{n^2}{2}\left[5n^2 + 1 - 3l(l+1)\right] \tag{3.49}$$

In this regime, the interaction potential between two atoms separated by a distance R can be expressed as an Laurent series in R,

$$V\left(\mathbf{r}_1, \mathbf{r}_2\right) = \frac{1}{|\mathbf{r}_1 - \mathbf{r}_2|} = -\sum_{n=1}^{\infty} \frac{C_n}{R^n} \tag{3.50}$$

The first two terms of the series correspond to the Coulomb and charge-dipole interaction, respectively, and therefore vanish for neutral atoms. The first contribution therefore comes from the dipole-dipole interaction, which is given by

$$V\left(\mathbf{r}_1, \mathbf{r}_2\right) = \left(1 - 3\cos^2\vartheta_{ij}\right)\frac{d_i d_j}{R^3} \tag{3.51}$$

where d_i and d_j are the electric dipole operators and ϑ_{ij} is the angle between the interatomic axis and the quantization axis of the atoms. The higher order terms can be expressed in terms of a series expansion involving spherical harmonics.

In the following we will concentrate on two atoms in the same s state $|r\rangle$, i.e., $n_1 = n_2 = n$. In this case, the main contribution comes from a single combination of p states $|r'r''\rangle = |n_1', p_1, n_2', p_2\rangle$. In the case of rubidium, we have $n_1' = n$ and $n_2' = n-1$, as the difference in the quantum defect for s and p states is close to 0.5. The energy difference between the states $|rr\rangle$ and $|r'r''\rangle$ is the Förster defect δ_F. Then, we can write the interaction Hamiltonian in the basis consisting of $|rr\rangle$ and $|r'r''\rangle$ as

$$H = \begin{pmatrix} \delta_F & \frac{d_{r'r'}d_{r''}}{R^3}\sqrt{D_\varphi} \\ \frac{d_{r'r'}d_{r''}}{R^3}\sqrt{D_\varphi} & 0 \end{pmatrix} \tag{3.52}$$

where the coefficient $D_\varphi = 3$ follows from the angular part of the dipole operators. The eigenvalues of the interaction Hamiltonian are

$$V_{int}(R) = \frac{\delta_F}{2} \pm \frac{1}{2}\sqrt{\delta_F^2 + 4\frac{(d_1 d_2)^2 D\varphi}{R^6}} \tag{3.53}$$

Define $V_{dd} = d_1 d_2/R^3$. For $V_{dd} \gg \delta_F$, we have

$$V_{int}(R) = \pm\frac{d_{r'r'}d_{rr''}}{R^3}\sqrt{D_\varphi} \tag{3.54}$$

As the dipole-dipole interaction is so strong that it mixes the electronic eigenstates, the interaction decays like $1/R^3$ even though the unperturbed eigenstates do not have a finite electric dipole moment. The other regime is where the atoms are so far apart that $V_d d \ll \delta_F$. Then we can perform a Taylor expansion of $V_{int}(R)$, obtaining

$$V_{int}(R) = \pm\frac{(d_1 d_2)^2 D_\varphi}{\delta_F R^6} \tag{3.55}$$

This interaction is a van der Waals interaction decaying like $1/R^6$. In the limit $R \to \infty$, the negative eigenvalue connects to the unperturbed state $|rr\rangle$. From this, we can read off the van der Waals coeffcient C_6 to be

$$C_6 = \frac{(d_1 d_2)^2 D_\varphi}{\delta_F} \tag{3.56}$$

Note that δ_F may be negative for certain combination of states, in this case the van der Waals interaction is repulsive. Consequently there is is a crossover from a resonant dipole interaction at short distances to a van der Waals interaction at large distances taking place at a critical radius r_c, which is given by

$$r_c = \sqrt[6]{\frac{4\,(d_1 d_2)^2}{\delta_F^2}} \tag{3.57}$$

There is a dramatic scaling of the van der Waals coefficient with the principal quantum number n. Each transition dipole moment scales as $d_i \sim n^2$, resulting in a n^8 dependence from the dipole matrix elements. However, the Förster defect has the same scaling as the energy splitting between neighboring Rydberg states, $\delta \sim n^{-3}$. Overall, this results in a scaling of the van der Waals coefficient like $C_6 \sim n^{11}$.

3.4.2 The Rydberg blockade mechanism

Here, we will consider a reonant laser field between two levels again, with a ground state $|g\rangle$ and an excited Rydberg level $|r\rangle$. We will also assume that the atoms are far apart and that we can approximate the interactions as van der Waals interaction, that is, the atoms are separated by more than r_c. This system is fully described by the states $|gg\rangle$, $|gr\rangle$, $|rg\rangle$, and $|rr\rangle$. The Hamiltonian in this basis is of the form

$$H = \frac{\Omega}{2}(|g\rangle\langle r| \otimes 1 + 1 \otimes |g\rangle\langle r| + \text{H.c.}) - \frac{C_6}{R^6}|rr\rangle\langle rr| = \frac{\Omega}{2}(|gg\rangle\langle gr| + |gg\rangle\langle rg| + |gr\rangle\langle rr| + |rg\rangle\langle rr| + \text{H.c}) - \frac{C_6}{R^6}|rr\rangle\langle rr| \tag{3.58}$$

Note that the state $|-\rangle = (|gr\rangle - |rg\rangle)/\sqrt{2}$ is an eigenstate of the Hamiltonian with an eigenvalue of zero, and hence, does not take part in the ddynamics. So, we approximate our system as an effective three level system with the states $|gg\rangle$, $|+\rangle = (|gr\rangle + |rg\rangle)/\sqrt{2}$ and $|rr\rangle$. In this basis, the Hamiltonian is

$$H = \frac{\sqrt{2}\Omega}{2}(|gg\rangle\langle +| + |+\rangle\langle rr| + \text{H.c.}) - \frac{C_6}{R^6}|rr\rangle\langle rr| \tag{3.59}$$

In the weakly interacting regime where $|C_6|/R^6 \ll \Omega$, the system will undergo slightly perturbed Rabi oscillations with Rabi frequency Ω, but the qualitative picture is similar to the single atom case. However, in the strong interacting regime $|C_6|/R^6 \gg \Omega$, the first excitation from $|gg\rangle \to |+\rangle$ is unaffected by the interaction, while the second excitation from $|+\rangle \to |rr\rangle$ is off-resonant because of the strong interaction. One can see that the level $|+\rangle$ is just the EIT first excited state in the dressed state picture, while the state $|rr\rangle$ is the second excited state in a ladder type of configuration. This essentially means that the $|rr\rangle$ state is decoupled from the dynamics, as it can never be reached. This decoupling of the doubly excited state is called the "Rydberg blockade". We can reduce the description to a two level system consisting only of $|gg\rangle$ and $|+\rangle$, governed by the Hamiltonian

$$H = \frac{\sqrt{2}\Omega}{2}(|gg\rangle\langle +| + \text{H.c.}) \tag{3.60}$$

The dynamics of this Hamiltonian again produces Rabi oscillations, however with two important differences to the non-interacting case. First, the maximum probability to find an atom in the Rydberg state, p_r is $1/2$, as the $|+\rangle$ state has only one of the two atoms in the Rydberg state. Second, the Rabi frequency is enhanced by a factor of $\sqrt{2}$, resulting in

$$p_r(t) = \frac{1}{2}\sin^2(\sqrt{2}\Omega t) \tag{3.61}$$

The distance at which the blockade sets in can be determined by setting the interaction strength equal to the Rabi frequency. This results in a blockade radius r_b given by

$$r_b = \sqrt{\frac{|C_6|}{\Omega}} \tag{3.62}$$

The $|+\rangle$ state can be shown to be a maximally entangled state and if we can prepare our system in the $|+\rangle$ state using a pulse of duration $t = \pi/\sqrt{8}\Omega$, Rydberg atoms can be employed as qubits in a quantum computer.

3.4.3 Rydberg blockade as a nonlinear medium

The shift in a Rydberg Level is given by

$$\Delta_{Ryd} = -\frac{1}{2}\frac{\alpha\varepsilon^2}{\hbar} \tag{3.63}$$

where α is the atomic polarizabilty at the frequency of the external field, whose amplitude is given by ε, which, depending on the system, can be different from the laser field. The low frequency susceptibility scales with the principal quantum number n as n^7. To qualitatively understand the Rydberg–Rydberg interaction, consider that another Rydberg atom produces a low frequency field ε proportional to the induced Rydberg dipole which scales as n^2. Considering only the dipole-dipole interaction term in the interaction Hamiltonian, we obtain a scaling $\alpha\varepsilon^2 \sim n^{11}$, which is like a Van-der-Waals interaction, as shown in a previous subsection.

The nonlinearity of a Rydberg blockade can be expressed as a third-order nonlinearity like the Kerr Effect, as

$$\chi^{(3)}\varepsilon^2 = \frac{\partial\chi_r}{\partial\omega}\Delta_{Ryd} = -\frac{n_g\alpha}{\omega}\varepsilon^2 \tag{3.64}$$

where χ_r is the real part of the electric susceptibility, $n_g = 1 + \omega\frac{\partial n}{\partial\omega} \simeq \frac{1}{2}\omega\frac{\partial\chi_r}{\partial\omega}$ (for large group index, for example, in a dilute medium with refractive index close to unity, or, in an EIT).

The term **Rydberg blockade** refers to the case where the interaction-induced shift is much larger than the EIT linewidth. The volume around a Rydberg atom in which the EIT is suppressed, that is, where the atoms can carry out the transition from the ground state to the first excited state but not the EIT transition from the first excited state to the second excited state, is called the Rydberg blockade, which has been mathematically demonstrated in the last subsection. This can roughly be taken as the region in which the Van-der-Waals interaction has a very dominant influence. As already mentioned, an atom-light quasi-particle is also called a polariton. The Rydberg blockade forms what is known as a **dark state polariton**-dark state in the sense that the EIT control beam passes through without getting absorbed just like seen in a dark state. However, as we are monitoring the probe beam, we will only see the transparency due to the EIT.

We can derive the blockade radius r_b in another way. In the case of the Rydberg blockade, the nonlinearity can be considered as a switch from the 3-level EIT susceptibility $\chi_{3-level}$ to the 2-level susceptibility $\chi_{2-level}$. The Rydberg Blockade Radius can be found from the requirement that $V(r_b) = 2\hbar\Gamma_{EIT}$, where V is the Rydberg-Rydberg interaction potential. For a Van-der-Waals interaction, $V(r) = C_6/r^6$. So,

$$r_b = \sqrt[6]{\frac{C_6}{2\hbar\Gamma_{EIT}}} \tag{3.65}$$

The nonlinear effect is more pronounced for more atoms contributing to the 2-level susceptibility within the blockade sphere. So, the nonlinearity is more for more optical depth per blockade sphere. However, even in the classical or partially blockaded regime, the nonlinearities are about five orders of magnitude higher than the normal EIT medium. For calculating this, let us first relate the two and three-level nonlinearities. Rydberg excitation converts a fraction $(\frac{\Omega_p}{\Omega_c})^2$ of nearby atoms to 2-level scatterers. So,

$$\chi_{3-level} = N\frac{4\pi}{3}r_b^3\left(\frac{\Omega_p}{\Omega_c}\right)^2\chi_{2-level} \tag{3.66}$$

Now, $\Omega_p = d\varepsilon_p/\hbar$, where d is the dipole matrix element for the 2-level transition. This gives a Kerr-like nonlinearity. For a blockade radius of 5 µm and a control Rabi frequency (Ω_c) of a few MHz, and typical atomic density as in a thermal vapour cell, the nonlinearity can be calculated to be almost 5 orders of magnitude higher. Similarly, the Rydberg EIT can be shown to have a dispersive quantum nonlinearity.

The Rydberg EIT has been used to produce various kinds of non-classical light states. As has already been mentioned in the Introduction, Rydberg polaritons are a potential candidate for various kinds of quantum simulation. Most mention-worthy out of all the non-classical light experiments is probably the work done in Vladan Vuletic's group at MIT, where they have recently shown three photon bunching using a Rydberg EIT medium [36]. Previously, two photon bunching has been shown [15]. Our experiments are motivated from these experiments proving the non-linearity of the EIT medium.

We tried to obtain squeezed light from a Rydberg EIT medium. Rather, we have tried observing the EIT probe-beam emerging from the vapour cell using a balanced homodyne setup, and have obtained some preliminary signs of phase dependent noise, which might be indicative of quadrature squeezing. This could be a very useful alternative to conventional media which can produce squeezed light, like an Optical Parametric Oscillator (OPO) [37], which has been shown to produce highly squeezed states[31] [38]. OPOs also have a second order nonlinearity, which can be obtained from the Rydberg blockade as discussed above. Although the squeezing we have obtained is not as much as obtained from OPO setups, this is a preliminary result and the results can be improved using cold atoms, for which we can expect higher optical depth per blockade volume. Details of the experiment shall be provided in later sections.

4

Experimental details, results and analysis

In this chapter, I will detail out my experimental setup and provide a step by step methodology for our experiments, both at Uni Mainz and at IISc. The experiments were very similar and so were the setups, although the end goal was different. At IISc, as already mentioned in the Introduction, we have been able to reach different n states for the Rydberg EIT, upto $n \simeq 60$, after which we have faced some problems regarding the resources that we have. This is rather similar to what we did in Mainz as an initial step, that is, progressively go up in n states so that the Rydberg blockade size increases, observe the EIT first, and then measure the shot noise in the different quadratures for the probe beam emerging out of the EIT. In Mainz, we have been able to go upto $n = 95$, where we have observed some splitting of the EIT peak, which justifies that what we have been trying here at IISc is possible at high enough n levels.

We have worked with diode lasers at both places. At Mainz, we worked with Toptica diode lasers, which were pre-set-up and already working when I started my project. I had to set up and use frequency stabilisation schemes for the three lasers that were being used for my experiment. There were two main lasers, which were used for obtaining the Rydberg EIT in the Homodyne Detection Setup. These were drawn with single mode polarisation maintaining fibers from their respective locking schemes, which I shall describe in detail. A third laser was drawn using a fiber into the blue laser locking setup for locking the blue laser with a Rydberg EIT itself. This laser was locked at a different optical table with a technique called SAS, which is something I will describe in a while.

At IISc, I was working with a 480 nm Toptica diode laser but the 780 nm laser was home built. This meant that I got the opportunity to set the laser up from scratch, which was a huge learning experience. I shall start by describing this process.

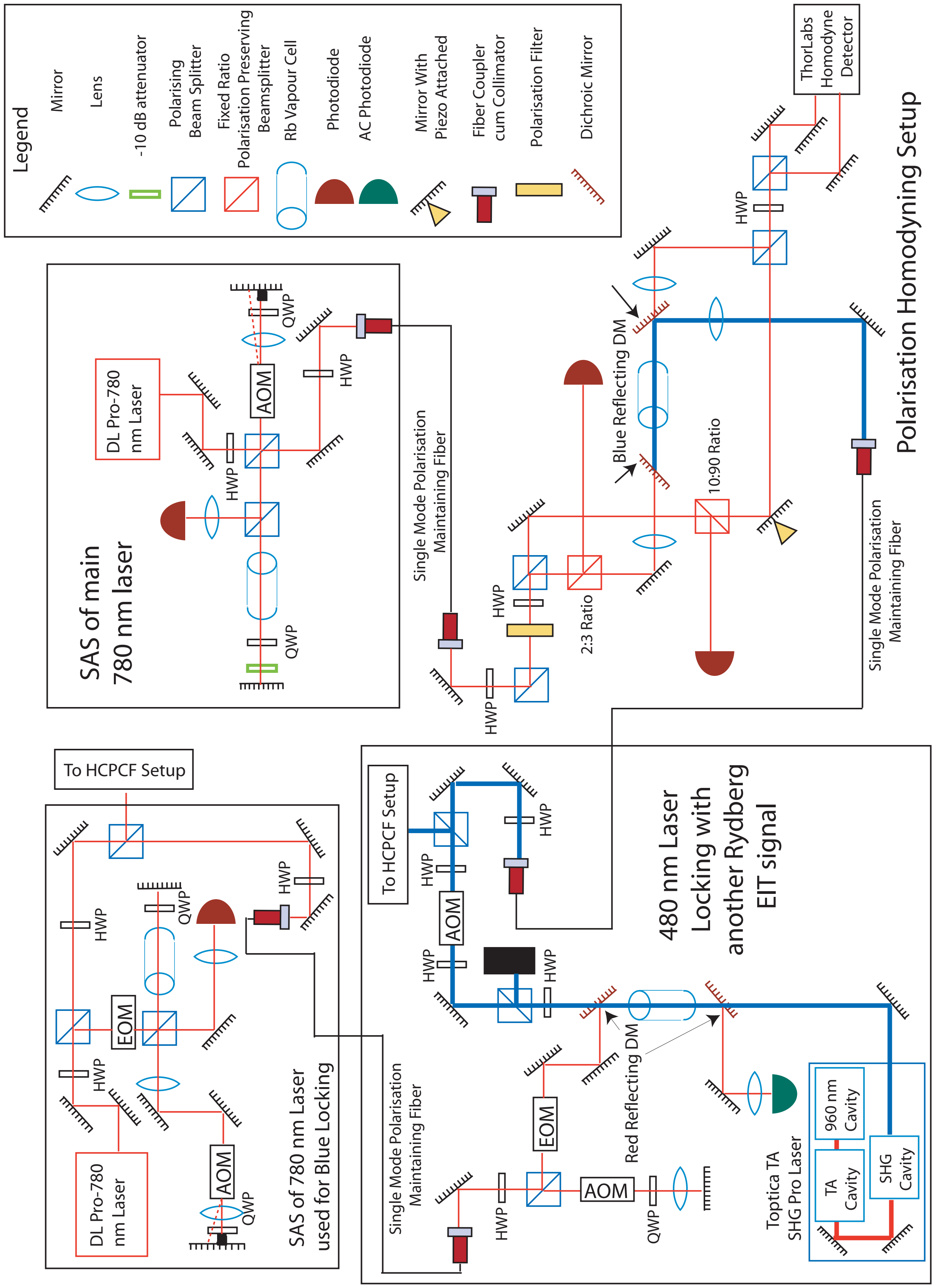

Figure 4.1: Schematic of experimental setup for balanced homodyne detection of squeezing from Rydberg EIT

4.1 Setting up an external cavity diode laser

We start by wearing a metal wrist band and grounding ourselves so that any static charges are not transferred to the laser diode. All tools used should be kept on an insulating mat to prevent any static charge accumulation, after they are grounded once. Now, as is customary while installing any new device, we carefully look at the specifications of the diode data sheet and identify the maximum optical power P_{max}. We check the pin codes of the diode and the jumper settings are set according to it. The switch is made positive/negative in the current controller according to the jumper settings.

Next we do what is called the open loop measurement. We measure the power vs the current at the controller and calibrate this, without putting in the grating. We put the current corresponding to the maximum power as I_{max} in our current controller to avoid any problems. The diode is usually operated at $0.9P_{max}$. The beam coming out of the laser diode is usually slightly elliptical and we do beam profile measurements with a ThorLabs Optical Beam Profiler to calculate the Rayleigh Range and other such parameters for the Gaussian beam. We also measure the threshold current. Next we put in the diffraction grating that is the key tool in controlling the wavelength of our laser. Once we put in the grating, we go to current levels slightly above the threshold level. The grating is usually set up in the Littrow or Blazed Grating configuration, in which the reflection and the diffraction orders are merged so that the laser gets feedback properly. The brightest spot coming from the grating is the 0^{th} order and the next spot is the ± 1 order. We see the $+1$ order next to the 0^{th} order, and we make the two coincide for obtaining flashing. The -1 order goes back inside the laser cavity and when we match the other two orders, the -1 order exactly retraces the 0^{th} order upon reflection. We use a CCD camera to monitor this on a dark background. We play with the grating angle and height and merge these orders. When they merge, there is a sudden increase in brightness of the spot, which is called flashing. For our laser, flashing was obtained at 29 mA of current. We usually operate our laser at current levels around 100 mA. Flashing at a low enough level would mean that the laser would have good feedback at high current levels and that we would not expect too many mode hops.

After this, we fix the grating and we direct our beam into the wavemeter. then, for coarse adjustment, we play with the grating angle to get near the necessary wavelength. For fine adjustment, we have a piezo attached to the grating which can change the distance of the grating from the diode lens and hence the orientation very slightly. This can change the wavelength in small steps. Then, once we are near the required wavelength for the atomic transition, we try and get the fluorescence of our atomic medium. Once we observe the fluorescence, we set up the SAS, which has been described in the next section.

The experimental setup has been described in Fig. 4.1. The different parts of the setup have been labelled accordingly. It consists of four parts, each connected to the others by single mode polarisation maintaining fibers-the SAS locking scheme for 780 nm laser used as EIT probe for the blue locking, the blue locking scheme, the SAS locking for the 780 nm laser used as EIT probe for Homodyne setup, and the Homodyne setup itself.

4.2 Frequency stabilisation of the laser

4.2.1 Saturated absorption spectroscopy

Lasers, in general, are non-equilibrium dynamic systems which need active feedback to stay at a certain frequency. Atomic transitions require narrow linewidth of lasers and transitions of narrow linewidths can often not be seen because of various kinds of broadening of the spectrum. The most prominent among these is Doppler broadening. Doppler broadening occurs because different velocity groups perceive different frequency shifts due to the Doppler effect. We can approximate that the atoms follow a Maxwell Boltzmann Distribution in a thermal vapour cell given by

$$n(v)dv = N\sqrt{\frac{m}{2\pi k_B T}}e^{-\frac{mv^2}{2k_B T}}dv \tag{4.1}$$

This results in a broad absorption profile which does not show the different hyperfine transition. In **Saturated Absorption Spectroscopy (SAS)** we use a strong pump beam and a weak probe beam of the exact same frequency (often, we just retro-reflect the pump after passing it through some attenuator) and align them with each other inside the atomic medium. They are usually made counter-propagating. Since the transition probability increases nonlinearly with respect to the light intensity and the pump beam is strong, we can expect that some electrons are pumped to the excited state when the laser field is resonant with a transition. This population transfer leaves fewer atoms in the ground state than before and the weak probe beam passes through with less absorption. This happens for two reasons-the transition probability for the weak probe is very less, and there are very few electrons in the ground state left to absorb photons. So very few photons are absorbed and we see heightened transmission, essentially, a peak in transmission at the resonant frequencies. We know that at the saturation intensity I_{sat}, the population is 25% in the excited state. Usually, we operate at powers of the pump beam lower than this value. We can calculate I_{sat} as

$$I_{sat} \equiv \pi hc/3\lambda^3\tau \tag{4.2}$$

We can also use a very practically applicable formula for calculating the Rabi frequency of a certain transition.

$$2\frac{\Omega^2}{\Gamma^2} = \frac{I}{I_{sat}} \tag{4.3}$$

These are hyperfine peaks for the zero velocity atoms. But the field also interacts with the non-zero velocity atoms and show what are called "crossover" peaks. These peaks arise at exactly the middle of 2 transition frequencies. Here, the pump is resonant with one transition and the probe is resonant with another transition, probabilistically speaking. So both positive and negative velocity groups contribute to the crossover peak and hence they are more prominant than the resonance peaks. Typical SAS spectrum for ^{87} Rb is shown in Fig. (4.2). This signal has been obtained after subtracting the Doppler background from the SAS spectrum. In the experimental setup Fig. (4.1), one can see the experimental setup for a SAS, where we send counter propagating strong pump and weak probe after retro-reflection through an attenuator. The Quarter Wave Plates (QWP) are used for phase correction after reflection from the mirror as we are using a double pass configuration for the AOM. These shall be briefly described in the next section.

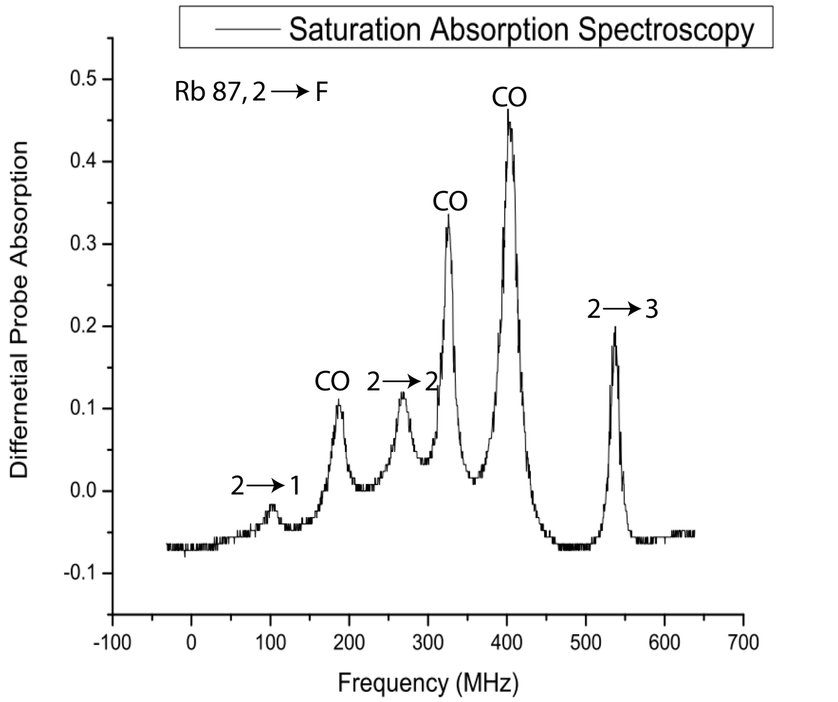

Figure 4.2: ^{87}Rb D_2 line $F_g = 2 \rightarrow F_e$ SAS spectrum

4.2.2 Some experimental techniques and devices used in our setup

Acousto-Optic Modulator-This has been referred to as AOM in our experimental setup. AOMs are devices used for frequency shifting a certain laser beam by a value, usually in 10s of MHz. It consists of a crystal to which an RF signal is fed. This creates phonon based acoustic vibrations in the crystal which forms a dynamic grating by a "Raman-Nath" like effect. The beam is either upshifted or downshifted depending on which order of diffraction we select, and depending on the direction of the RF signal fed into it. AOMs can also be used for intensity manipulation of a certain order. The orders are deflected by a certain angle depending on the magnitude of the RF waves. The angle of the AOM with the beam also determines how many orders of diffraction in which direction are generated.

To take care of this problem of the AOM upshifted or downshifted beam emerging at an angle with the original beam, people often use what is called the "Double-Pass Technique". In this technique, we use a convex lens or a concave mirror after the AOM. If a convex lens is used, both the AOM and the mirror are placed at the focii of the lens. The first order diffraction is usually selected and the zeroth order is blocked. This first order upon reflection from the mirror again gets either upshifted or downshifted (depending on whether we select $+1$ or -1 order) and retraces the beam path of the original beam. Thus, if we set a frequency f that the AOM will shift the beam by in every pass, the beam gets frequency shifted by $2f$, while maintaining the original beam direction. This way, we can use the AOM for frequency scanning as well.

Electro-Optic Modulator-This similar to an AOM but driven by the electrical signal from a function generator. It works on the electro-optic effect, where the refractive index depends on the electric field. It is used for electrical modulation of the beam. This generates sidebands for a laser beam, which can be used for locking the laser, which has been discussed in the next subsection. The sideband spacing is equal to the driver frequency. In our setup, we have given a 9.3 MHz signal to our EOM.

Vapour Cells-We have used a pure cell for our experiments where there is 72% ^{85}Rb and 28% ^{87}Rb, although we have only used ^{87}Rb for our experiments. The cell is a cylinder with dimensions of 25 mm dimater and 50 mm length. At room temperature, the vapour pressure is 3×10^{-7} torr.

4.2.3 Generating error signals and locking the laser

Let me motivate this section by first outlining a general theory for generating error signals from a Pound Drever Hall (PDH) Driver. For generating a PDH readout, we modulate the signal from a PD with some sort of external electric field. Consider a field $E_0 e^{i\omega t}$ and this is phase modulated by some $\beta \sin \omega_m t$. The resulting field E_i is

$$\begin{aligned} E_{\mathrm{i}} &= E_0 e^{i(\omega t + \beta \sin(\omega_{\mathrm{m}} t))} \\ &\approx E_0 e^{i\omega t}\left[1 + i\beta \sin\left(\omega_{\mathrm{m}} t\right)\right] \\ &= E_0 e^{i\omega t}\left[1 + \frac{\beta}{2} e^{i\omega_{\mathrm{m}} t} - \frac{\beta}{2} e^{-i\omega_{\mathrm{m}} t}\right] \end{aligned} \tag{4.4}$$

This field may be regarded as the superposition of three components. The first component is an electric field of angular frequency ω, known as the carrier, and the second and third components are fields of angular frequency $\omega + \omega_m$ and $\omega - \omega_m$, respectively, called the sidebands. Consider the cavity formed by the AOM and the reflecting mirror during double pass. In general, this can be replaced by any sort of Fabry-Perot cavity. The light

E_r reflected out of a Fabry–Pérot two-mirror cavity is related to the light E_i incident on the cavity by the following transfer function:

$$R(\omega) = \frac{E_\mathrm{r}}{E_\mathrm{i}} = \frac{-r_1 + (r_1^2 + t_1^2)\, r_2 e^{i2\alpha}}{1 - r_1 r_2 e^{i2\alpha}} \tag{4.5}$$

where $\alpha = \omega L/c$, and where r_1 and r_2 are the reflection coefficients of mirrors 1 and 2 of the cavity, and t_1 and t_2 are the transmission coefficients of the mirrors. Applying this transfer function to the phase-modulated light E_i gives the reflected light E_r:

$$E_\mathrm{r} = E_0 \left[R(\omega) e^{i\omega t} + R\left(\omega + \omega_\mathrm{m}\right) \frac{\beta}{2} e^{i(\omega+\omega_\mathrm{m})t} - R\left(\omega - \omega_\mathrm{m}\right) \frac{\beta}{2} e^{i(\omega-\omega_\mathrm{m})t} \right] \tag{4.6}$$

The power P_r of the reflected light is proportional to the square magnitude of the electric field, $E_r * E_r$, which after some algebraic manipulation can be shown to be

$$\begin{aligned} P_\mathrm{r} =& P_0 |R(\omega)|^2 + P_0 \frac{\beta^2}{4} \left\{ \left| R\left(\omega + \omega_\mathrm{m}\right) \right|^2 + \left| R\left(\omega - \omega_\mathrm{m}\right) \right|^2 \right\} \\ &+ P_0 \beta \left\{ \mathrm{Re}[\chi(\omega)] \cos \omega_\mathrm{m} t + \mathrm{Im}[\chi(\omega)] \sin \omega_\mathrm{m} t \right\} + (\text{terms in } 2\omega_\mathrm{m}) \end{aligned} \tag{4.7}$$

Here $P_0 \propto |E_o|^2$ is the power of the light incident on the Fabry-Perot cavity, and χ is defined by

$$\chi(\omega) = R(\omega) R^*\left(\omega + \omega_\mathrm{m}\right) - R^*(\omega) R\left(\omega - \omega_\mathrm{m}\right) \tag{4.8}$$

This χ is the ultimate quantity of interest; it is an antisymmetric function of $\omega - \omega_m$. It can be extracted from P_r by demodulation. First, the reflected beam is directed onto a photodiode, which produces a voltage V_r that is proportional to P_r. Next, this voltage is mixed with a phase-delayed version of the original modulation voltage to produce V_r'

$$V_\mathrm{r}' = V_\mathrm{r} \cos\left(\omega_\mathrm{m} t + \varphi\right) \propto P_\mathrm{r} \cos\left(\omega_\mathrm{m} t + \varphi\right) \tag{4.9}$$

Finally, V_r' is sent through a low-pass filter to remove any sinusoidally oscillating terms. This combination of mixing and low-pass filtering produces a voltage V that contains only the terms involving χ:

$$V(\omega) \propto \mathrm{Re}[\chi(\omega)] \cos\varphi + \mathrm{Im}[\chi(\omega)] \sin\varphi \tag{4.10}$$

In theory, χ can be completely extracted by setting up two demodulation paths, one with $\phi = 0$ and another with $\phi = \pi/2$. In practice, by judicious choice of ω_m it is possible to make χ almost entirely real or almost entirely imaginary, so that only one demodulation path is necessary. $V(\omega)$, with appropriately chosen ϕ, is the PDH readout signal.

The error signal can be generated in two ways. One way is to pass the laser beam through an EOM as already mentioned to generate sidebands. Then the output of the photodiode is fed to a mixer where some signal is given from a function generator to the local oscillator in the mixer. Then the output of the mixer is fed to a Pound Drever Hall Unit, or, as in the case of blue locking, it is fed to a Fast Analog Control. From the Pound

Drever Hall Unit, which generates the error signal, the signal is fed to a PID controller. The PID controller does the actual locking in the sense that it always tries to bring the error signal to its zero.

The other way to generate the error signal is by using a current module, as in the case of the 780 nm main laser for Homodyne setup. The current module modulates the PD input and that is directly fed into the PDH driver. No EOM is required in this case. Then a similar path is followed. A FALC can perform a much faster lock compared to a normal PDH-PID lock. For operating a FALC, one feeds the signal directly from the mixer into the FALC. Some feedback is then turned on and one can see the feedback vary as one changes the piezo offset of the controller slightly. We locked both the lasers for our EIT in the Homodyne Setup, and then looked at the quadrature shot noise levels. The red laser was locked to the $F = 2 \rightarrow F' = 3$ transition in the D2 line of ^{87}Rb. The way we did this is we locked the laser to the $2 \rightarrow 3$ crossover. The double pass was adjusted to exactly upshift the beam so that it was at the $F = 2 \rightarrow F' = 3$ resonance. The error signal used for locking the blue laser is shown in Fig. 4.3.

4.2.4 Producing the blue light

The blue laser is produced from a 960 nm laser after passing it through a Second Harmonic Generation Cavity. Second Harmonic Generation is obtained from a nonlinear crystal by taking advantage of the second order nonlinearity of the crystal. The induced second-harmonic dipole per unit volume, $P^{(2)}(2\omega)$ is given by

$$E(2\omega) \propto P^{(2)}(2\omega) = \chi^{(2)} E(\omega) E(\omega) \tag{4.11}$$

The 960 nm laser is first passed through a Tapering Amplifier Cavity to amplify it and then passed through the SHG cavity. The laser produced can be at intensities upto 200 mW.

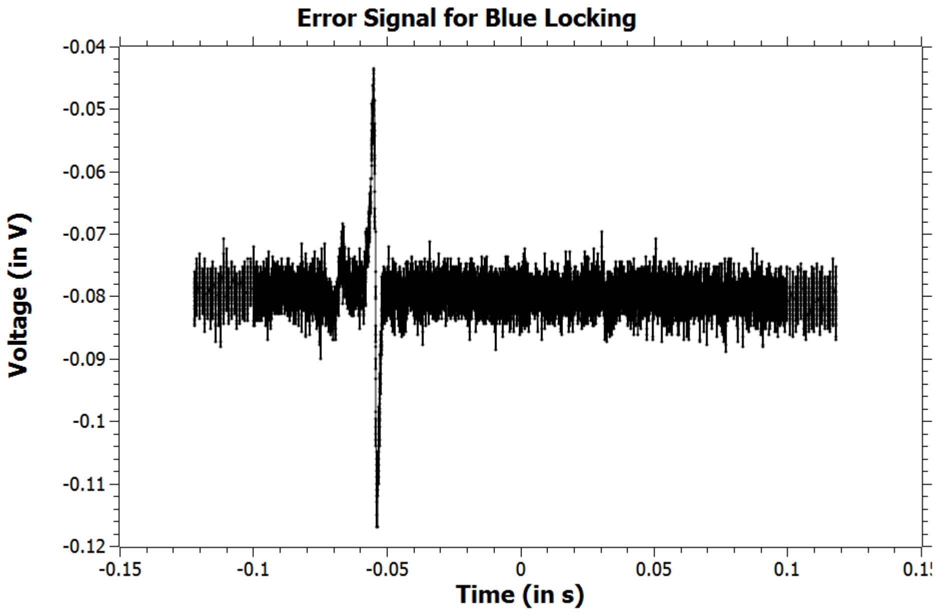

Figure 4.3: Error signal for 480 nm laser obtained from a Rydberg EIT at $n = 85$

4.3 Detector characterisation and automation of the setup

Let us first calculate exactly how the output variance would depend on the variance levels in the two quadratures and the intensities in the two arms. Consider light fields $|a\rangle$ and $|b\rangle$ incident on the beamsplitter at the beginning of a homodyne Setup. α and β are the mean values of the two fields. Let δa and δb be the uncertainties in the two fields. The quadrature is given by $X_\varphi = X_1 \cos\varphi + X_2 \sin\varphi$. The output field c and d are given by

$$c = \frac{1}{\sqrt{2}}(ae^{i\phi} + b) \tag{4.12}$$

$$d = \frac{1}{\sqrt{2}}(-ae^{i\phi} + b) \tag{4.13}$$

Then we can calculate the difference current as

$$I_- = c^+c - d^+d = 2\alpha\beta \operatorname{Cos}\varphi + 2\alpha\delta X^b_\varphi + 2\beta\delta X^a_\varphi \tag{4.14}$$

δX^a_φ and δX^b_φ are the total uncertainties for a and b for a certain quadrature value at an angle φ. Note that we are interchangeably using both c and d as operators for the coherent states and the coherent states themselves. As is obvious, the above expression calculates the photon numbers for coherent states $|c\rangle$ and $|d\rangle$. The variance in the signal is given by

$$\Delta^2 I_- = 4\alpha^2\Delta^2\delta X^b_\varphi + 4\beta^2\Delta^2\delta X^a_\varphi \tag{4.15}$$

Now, we know in any one arm, shot noise is proportional to the intensity. So

$$\Delta^2 I_{EIT} = mI_{EIT} + n \text{ and } \Delta^2 I_{LO} = pI_{LO} + q \tag{4.16}$$

So, we get

$$\Delta^2 I_{-} = \{4(m+p)I_{LO} + 4EN\}I_{EIT} + 4ENI_{LO} + EN \tag{4.17}$$

Finally, we can conclude

$$\Delta^2 V_{\mathrm{PD}} \propto P_{\mathrm{LO}} \Delta^2 X_{\phi}^{\mathrm{sig}} + P_{\mathrm{sig}} \Delta^2 X_{-\phi}^{\mathrm{LO}} \tag{4.18}$$

So, given two arms open, if the power of any one arm is kept constant, one would get a straight line for variance of homodyne output vs the intensity of the arm in which power is varied. If any one arm is open and the other arm is closed, we would see the vacuum field in the closed arm. So essentially, shot noise is way larger if both the arms are open. This would give us the shot noise limit value for the setup.

Our setup is a polarisation homodyning setup with two orthogonally polarised beams used in the two arms, which are mixed back at the mixing PBS. The reasons for polarisation homodyning are two-firstly it is much easier to operate a polarisation homodyning as one can get exact equal splitting at the homodyning PBS. Errors are, as a result, less. Secondly, according to a paper by Budker *et al*[39], linearly polarised light passing through a media where elliptically polarised light would show self-rotation, would show vacuum squeezing in the orthogonal polarisation to the linear polarisation. So we wanted to look at the polarisation only where the EIT is happening, so that we would know whether the squeezing is due to EIT alone or not.

Now, we initially took a lot of data but due to human error at various steps we were not getting very nice data. As in, our shot noise levels were not following the theoretically predicted trend. Also, we needed more data and faster acquisition. Due to all these factors, we have automated our setup. The automation has been carried out mainly by employing two motorized piezo-driven waveplate mounts (Fig. 4.4), which would move in a slip stick motion due to the piezo for smaller steps and jog with a stepper motor for larger steps. These mounts could be interfaced with a LabVIEW programme very easily. The power in the two arms of the homodyne setup were being monitored by splitting off the power with some constant ratio beamsplitters and then making some power fall on a photodiode. This photodiode was connected to an oscilloscope which could be operated with a LabVIEW VI. The LabVIEW VI would obtain the voltage levels from the different channels in the oscilloscope, which were characterised with respect to power. So, given a voltage level, we would know how much power was falling on the photodiode. Now, since the beamsplitters are constant ratio, we would know how much power is going into the setup, either in LO arm or EIT arm. The beamsplitters were thoroughly checked for any sort of non-preservation of polarisation but we did not find any. Once the power levels required are set, we would take the data. Until then, an active stabilisation would go on. We could in principle actively stabilise it even while taking data, but we found that the rotation of the mount led to increased acoustic noise in our signal.

The working of the LabVIEW code, although quite elaborate, is rather simple (Fig. 4.5). The code takes the voltage level from the oscilloscope and converts it to power in the respective arm as described above. Then this is compared to the required power as given by the user. The user has to input a lower limit and an upper limit for the power required. Then, there are two sets of loops, each corresponding to whether the power is less or more than the target value in that arm. For each result of the duality, there are two loops rotating the mount left or right, and constantly taking data about whether power is increasing or decreasing, and comparing it to what should happen. This is given by the flowchart below (Fig. 4.5). In Fig. 4.7, we have shown one such loop. There are four loops for each mount, and total eight loops, for two mounts.

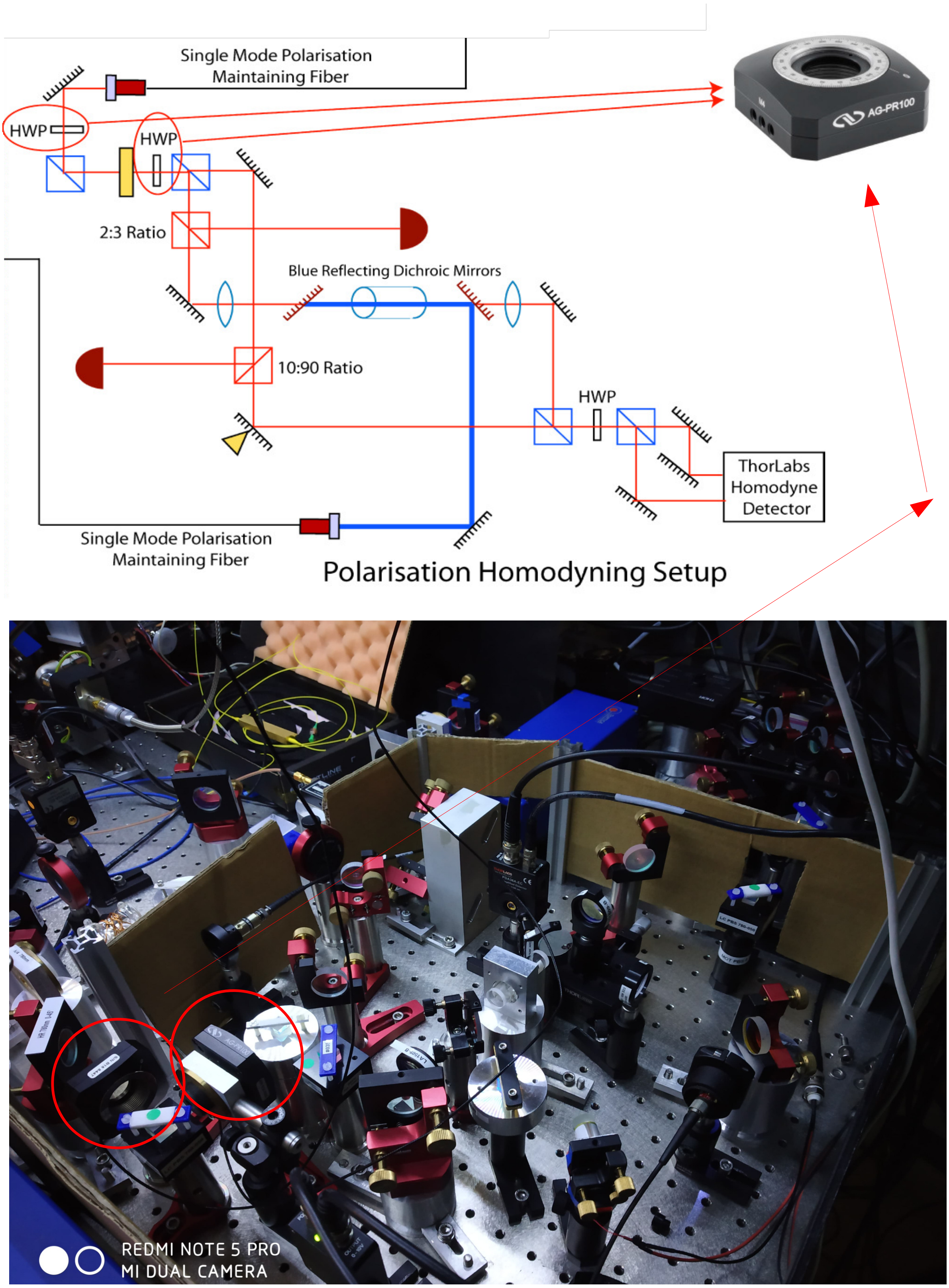

Figure 4.4: Balanced polarisation homodyning setup with piezo driven stepper motor rotation mount

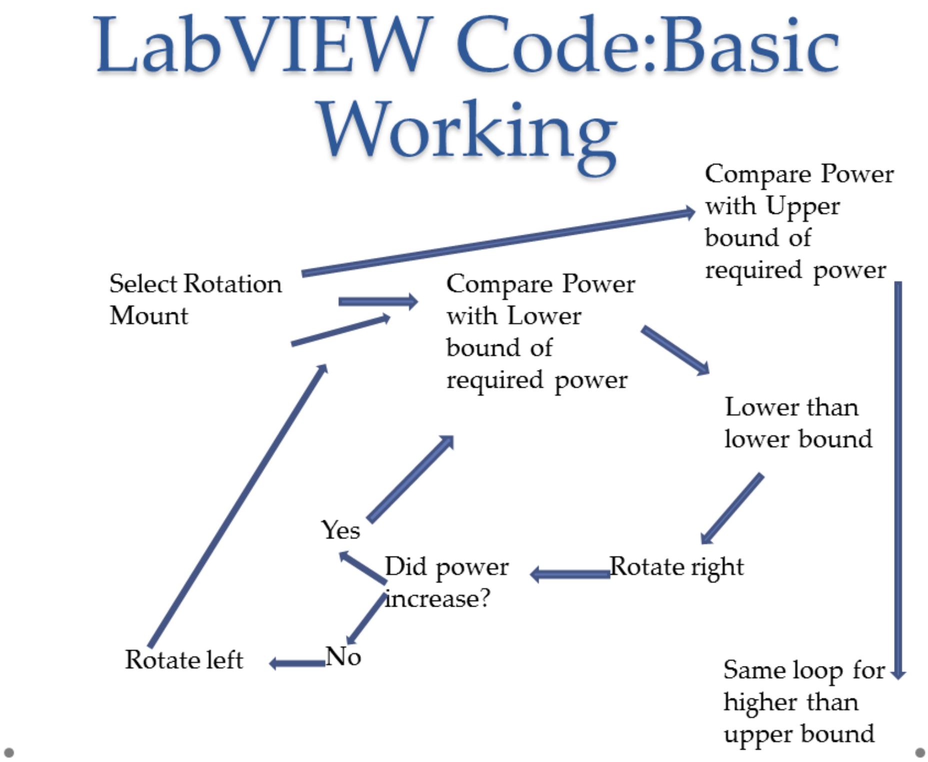

Figure 4.5: A basic flow chart of the LabVIEW code.

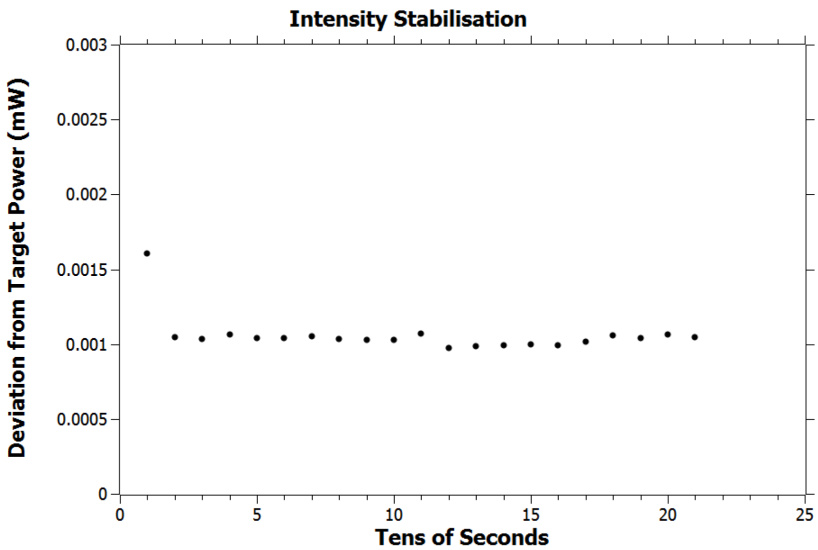

Figure 4.6: Intensity stabilisation achieved from automation. The error from target intensity level as measured by a power meter is shown.

As one can see from (Fig. 4.6), the Intensity stabilisation is rather efficient and can stabilise within 1 µW of error from target intensity value.

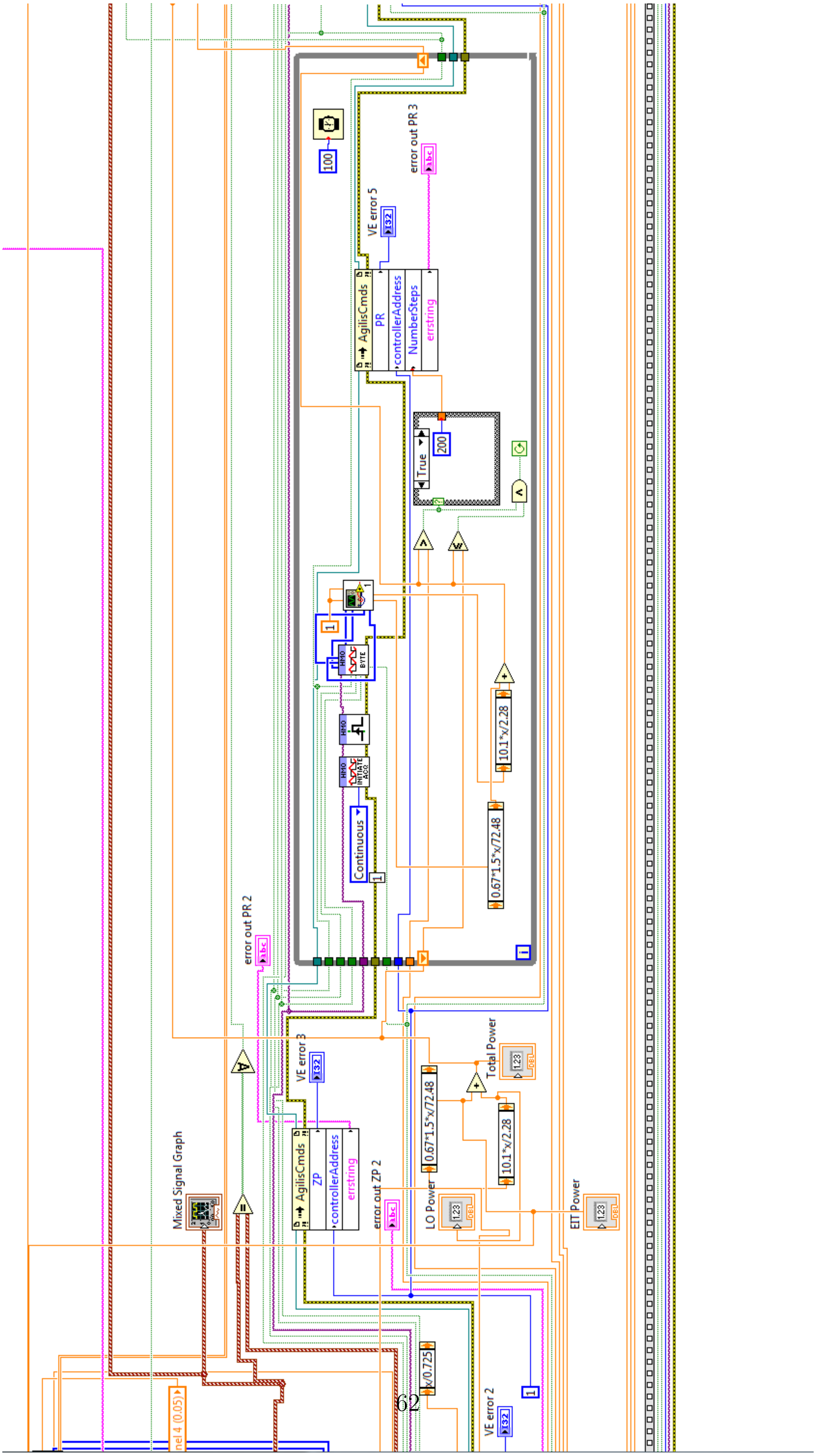

Figure 4.7: A fragment of the LabVIEW code demonstrating the loop usage

The characterisation data is then shown. First, we use a spectrum analyser in Zero Span Mode for characterising our setup (Fig. 4.8). Here, it displays noise level as a function of time at a constant frequency-which was 4 MHz in our case. The two arms show almost exactly identical data, and as predicted, follow a straight line. The noise level would depend on the Resolution BandWidth of our Spectrum Analyser, which was set at 100 kHz. In a finite span mode, i.e., 4MHz $\pm$ 200kHz, it showed similar results (Fig. 4.9 and Fig. 4.10). The higher the RBW, the higher would be the noise floor.

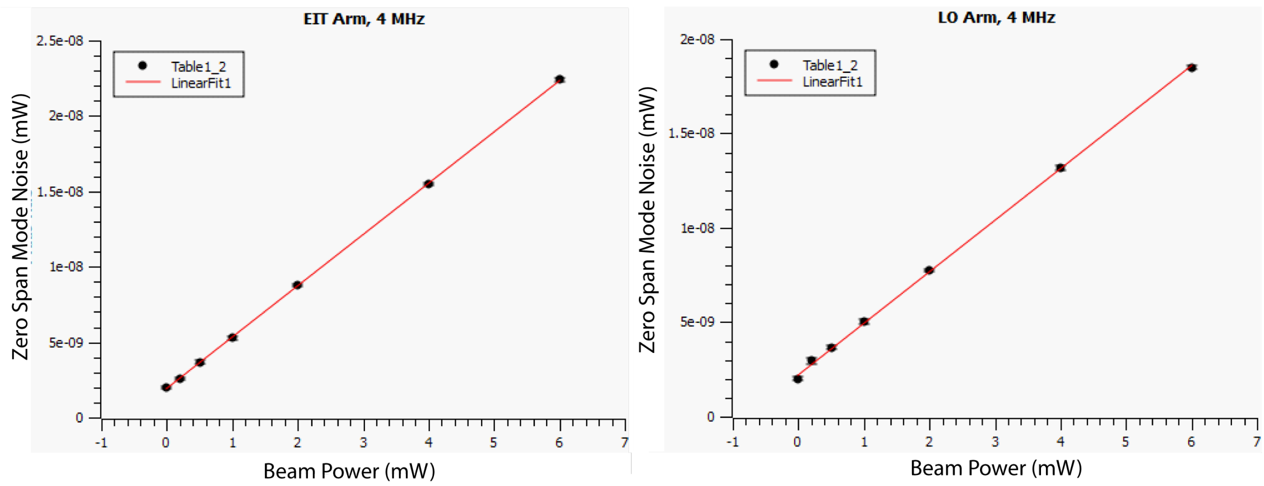

Figure 4.8: Characterisation of the setup with zero span mode of spectrum analyser with only one arm open.

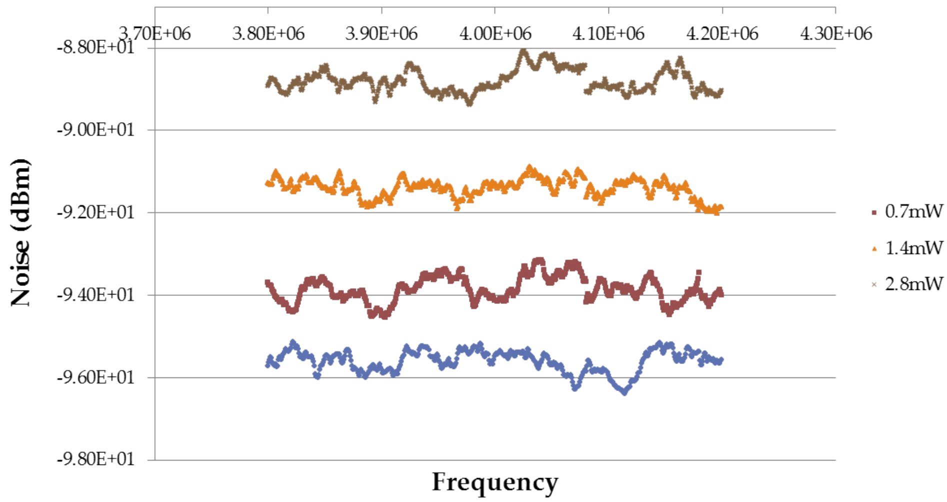

Figure 4.9: Traces as obtained from spectrum analyser for different power levels in 4 MHz $\pm$ 200 kHz finite span mode.

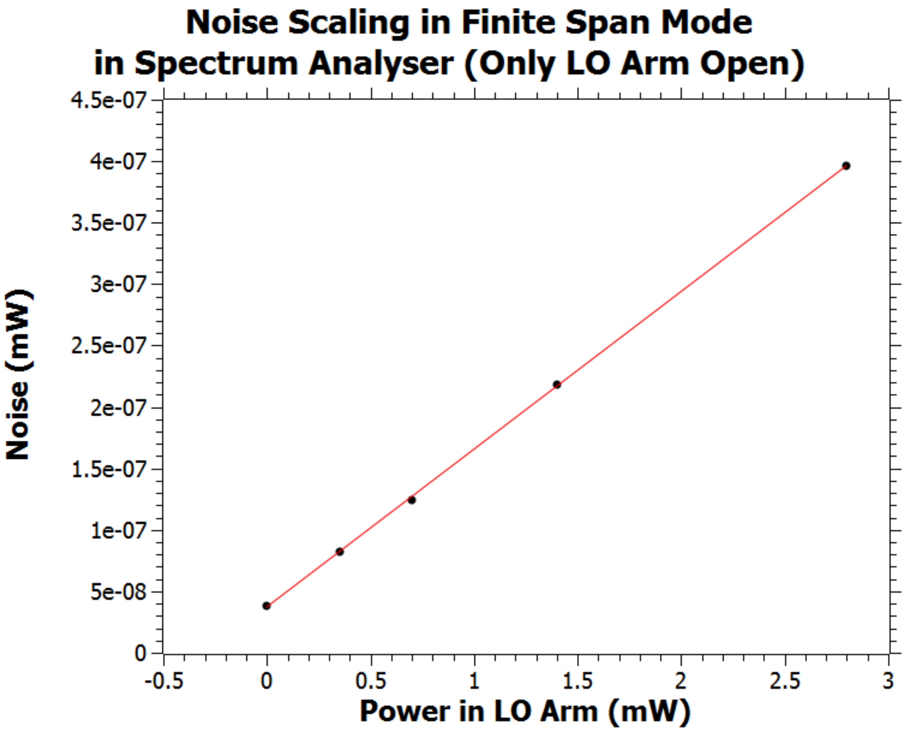

Figure 4.10: Noise as a function of power in finite span mode of spectrum analyser with only one arm open.

In our main experiment to detect squeezing, we have used data from a Lecroy oscilloscope. We have obtained the Homodyne Detector Output and then divided the obtained trace into bins of 0.25μs. This corresponds to 4 MHz, which we have used for characterisation using spectrum analyser. Then, we have plotted the variance for each bin and then calculated the average variance and the standard deviation. For a coherent state, the variance would be equal over all the bins theoretically. As already mentioned, coherent states are Gaussian states with constant variance. A phase shift in any of the two beams in the interferometer is essentially a displacement operation for a coherent state, or a look at a different quadrature. For a squeezed state, we would obtain phase dependent uncertainty in the shot noise levels. To prove that our system is indeed shot noise limited at all power levels above a certain value, we plot the average variance over the entire trace vs the beam power, for two cases-one arm open and both arms open. As we see theoretically, for one arm open, as we vary the power of that arm, we would get a linear dependence on the power if we plot the total noise, which is, the electronic noise, the little bit of classical noise that we have, mainly as acoustic noise, and the shot noise, as a function of the power. We do get that (Fig. 4.11). Theoretically, for both arms open, if the power of one arm is kept constant, the total noise varies linearly with the power in the other arm. This is shown experimentally in Fig. 4.12. This has been measured after automation with $\simeq 95\%$ mode match and without piezo scan.

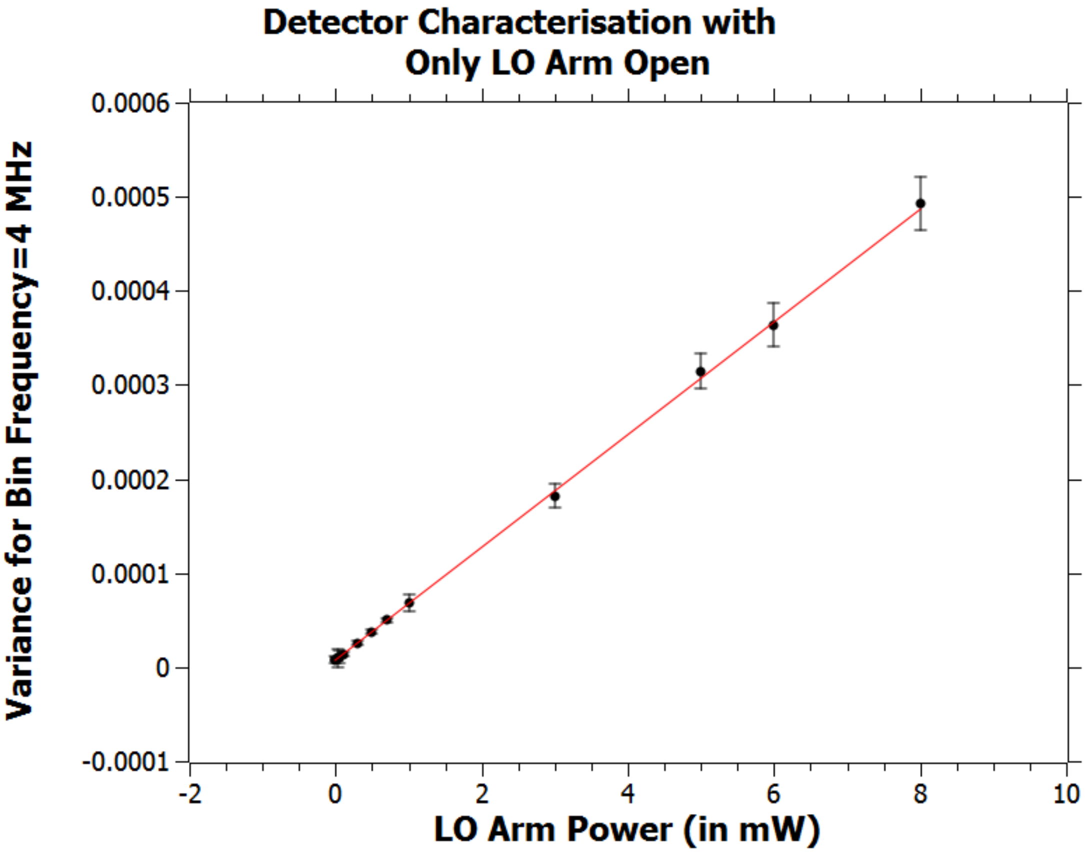

Figure 4.11: Detector characterisation after automation by measuring oscilloscope variance for bin number corresponding to 4 MHz, with only LO arm open.

From this graph, we find that our system is shot noise limited for all powers above $\simeq 350$ µW, with one arm open. The other arm, as mentioned before, has the vacuum field.

Visibility or mode matching percentage is defined as

$$\text{Visibility} = \frac{I_{\max} - I_{\min}}{I_{\max} + I_{\min}} \tag{4.19}$$

This measurement is taken for only one arm open. It is essentially a $G^{(1)}(x_1, x_2)$ type of measurement. For only one arm open, the Homodyne Signal would be a sinusoidal signal with the minimum at $y = 0$ for perfect mode match. The I_{max} and I_{min} values are max and min values of this sinusoidal signal. The mode match is first done by looking at a beam tracing camera. We can see the individual beams quite clearly. The two beams are brought together and then we play with two mirrors, the "mode-matching mirrors", to minimise interference between the two modes. This would mean that any fringes appearing when the beams are brought together would disappear. Then we look at the balanced Homodyne signal and maximise this visibility parameter. Our experiments were routinely done with visibility $> 90\%$. Usually, it was around 95-96%.

With both arms open, as seen theoretically, the variance would vary linearly if the power of one arm is kept constant and the power of the other arm is varied. We get such a graph experimentally as well. LO Arm has been kept constant at 6 mW while EIT arm power is varied, with a high mode match value (Fig. 4.12). From Fig. 4.11 and Fig. 4.12, we can get the regime where we will be shot noise limited. We see that when one arm is open, we are shot noise limited for powers around 350 µW. This means that for both arms open, we are shot noise limited at all power levels in the EIT arm, for a constant power of 350 µW and above in the LO arm. So, essentially, we are working in a regime where we are looking at only quantum noise and all fluctuations are quantum in nature. Any results we get in this regime would directly imply a change in the quantum state of our signal light field.

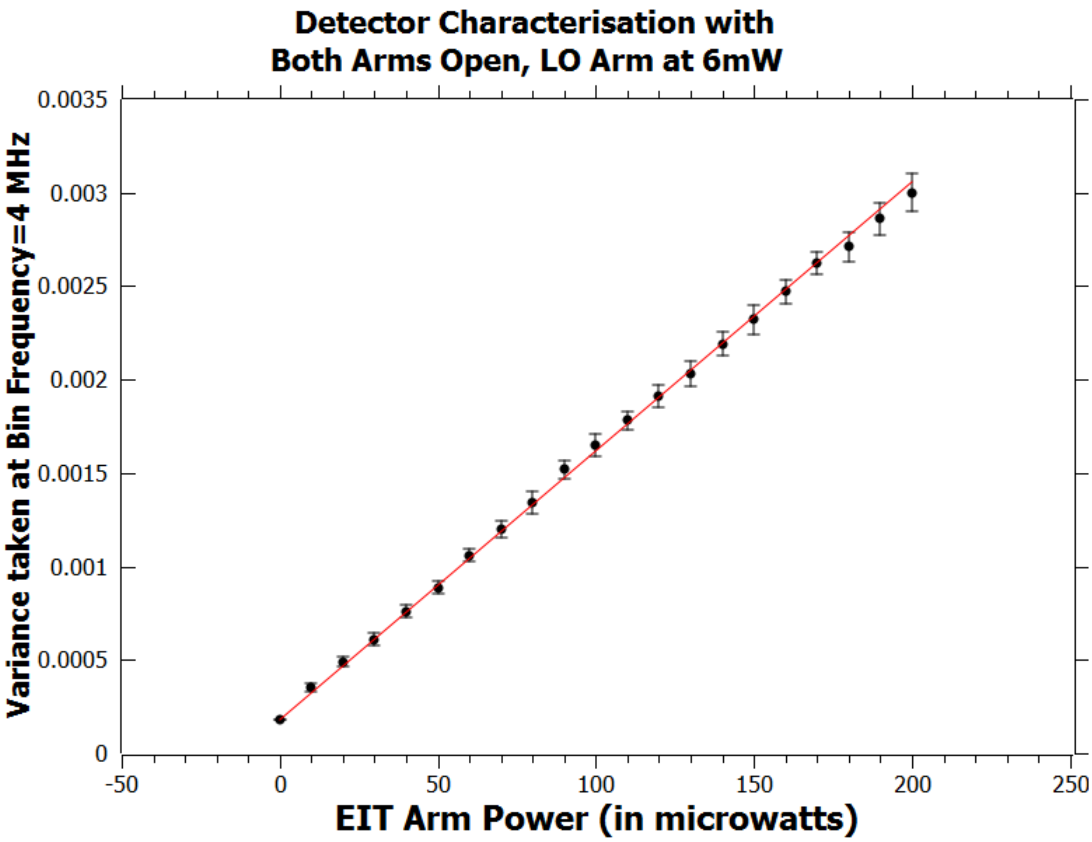

Figure 4.12: Detector characterisation after automation and $\simeq$ 95% mode match by measuring oscilloscope variance for bin number corresponding to 4 MHz, with both LO and EIT arm open.

4.4 Rydberg EIT at different n levels and the Rydberg blockade

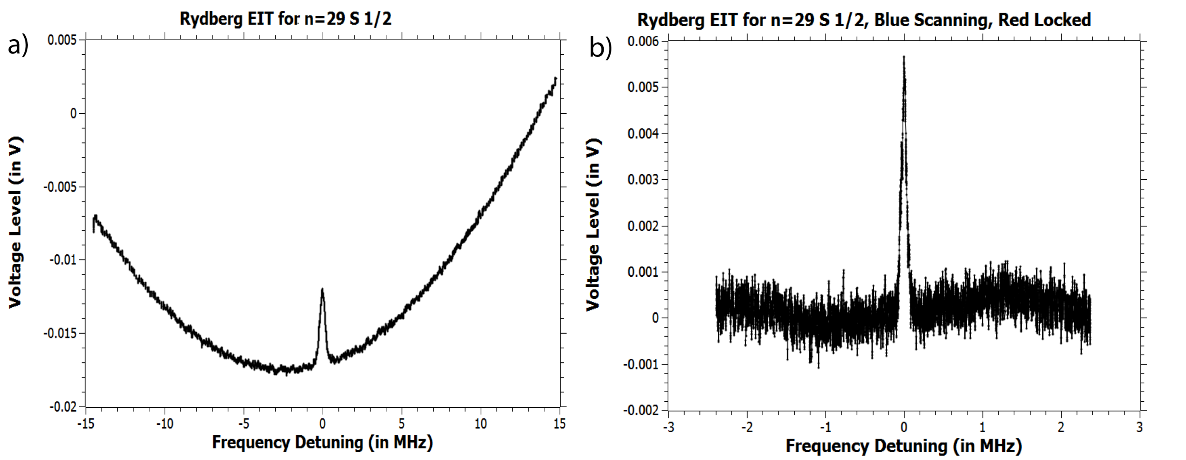

Figure 4.13: Rydberg EIT for $n = 29\,\mathrm{S}_{1/2}$. a) EIT with red scanning and blue locked to error signal from corresponding EIT in blue locking setup. b) EIT with blue scanning and red locked to 2 to 3 crossover peak of SAS.

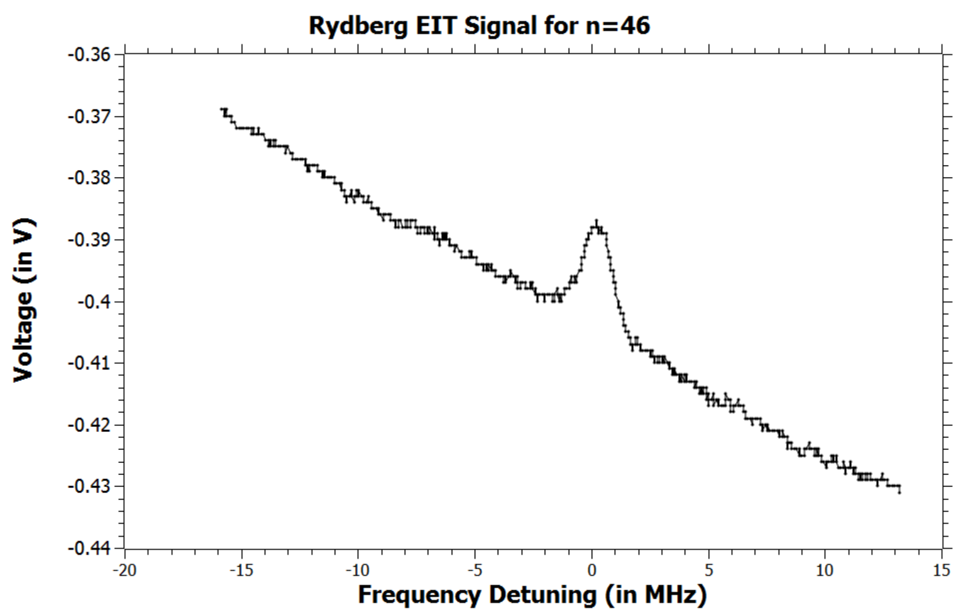

Figure 4.14: Rydberg EIT for $n = 46\ \mathrm{S}_{1/2}$ with red scanning and blue locked to corresponding EIT error signal.

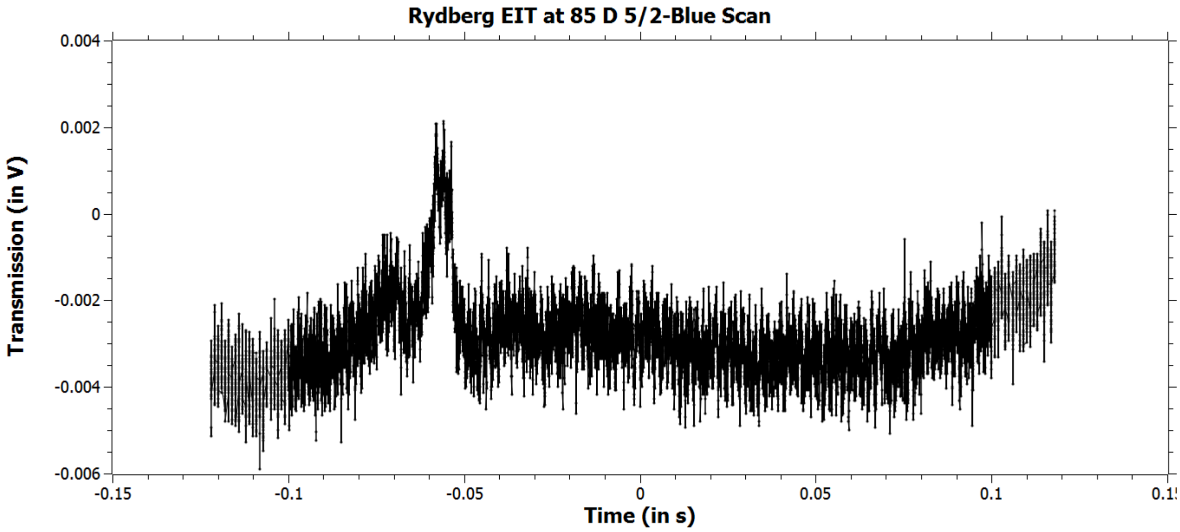

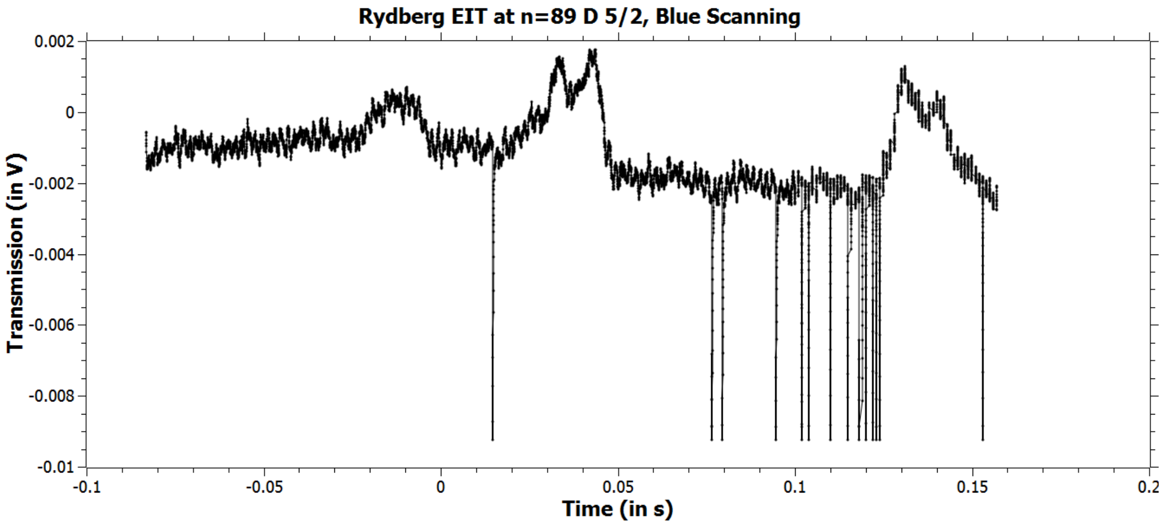

Figure 4.15: Rydberg EIT for a) $n = 85\,\mathrm{D}_{5/2}$ and b) $n = 89\,\mathrm{D}_{5/2}$, with blue scanning and red locked.

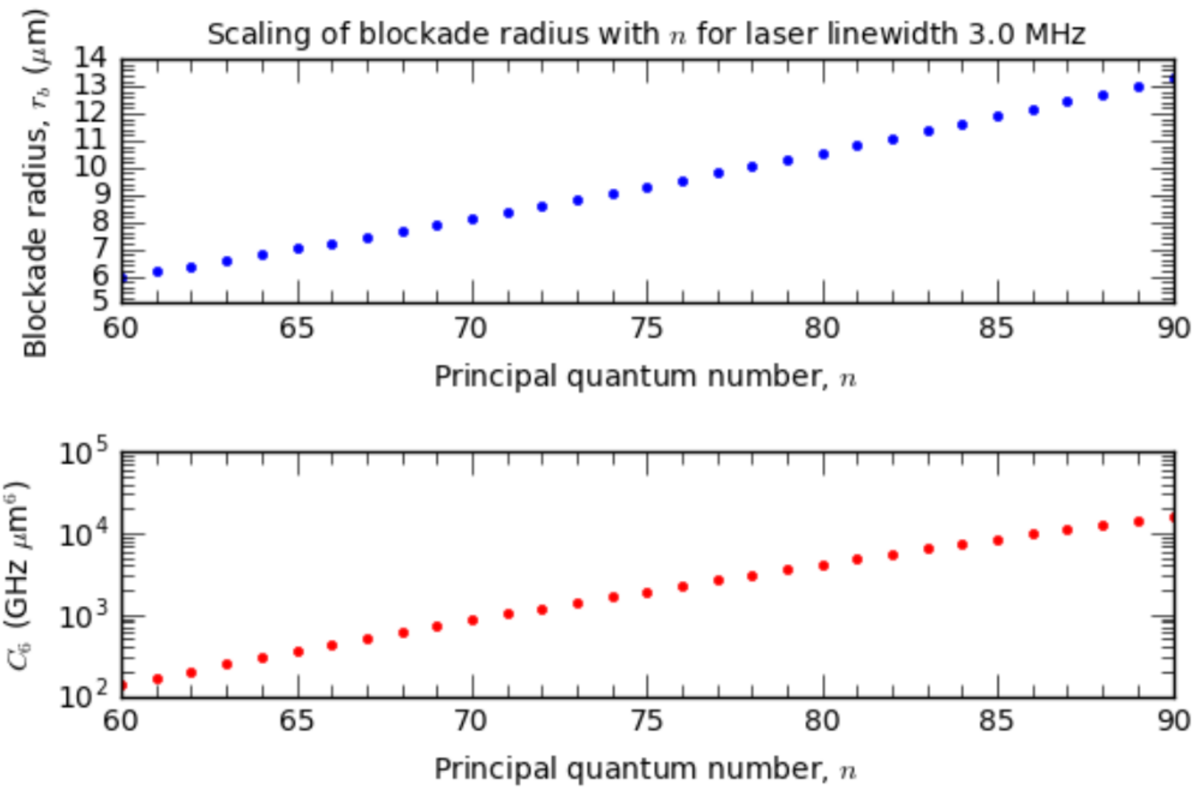

Figure 4.16: Graph showing the scaling of the Rydberg blockade with n value of the Rydberg transition.

In (Fig. 4.13) Linewidth=$2\pi \times 0.4$ MHz. Intensity of blue laser = 4.7746 mW/mm^2. Intensity of red laser = 9.55 µW/mm^2. In (Fig. 4.14), linewidth=$2\pi \times 1.3$ MHz. Intensity of blue laser = 10.186 mW/mm^2. Intensity of red laser = 9.55 µW/mm^2. In (Fig. 4.15), intensity of blue laser = 0.61 mW/µm^2. Intensity of red laser = 0.1 µW/µm^2. We have obtained Rydberg EIT signals for different n values. As the n increases, the signal amplitude in general decreases for the same Rabi frequencies of the probe and control. As control Rabi frequency decreases, we have sharper peaks. The amplitude of the peak increases both by increasing probe and control Rabi frequencies. We have obtained very narrow EIT signals, of linewidth $2\pi \times 0.4$ MHz at $n = 29$ $S_{1/2}$. As seen, for $n = 46$ as we increase the control Rabi, we have a much bigger EIT. Something really interesting happens for Rydberg EIT at very high n levels. As seen in (Fig. 4.15), at very high n levels, the EIT is very sensitive to external electromagnetic fields. These might be DC or AC fields. For a relatively lower magnitude of applied field, one would see a large shift in hyperfine levels of a Rydberg state. This would result in interesting effects like alternate EITs and EIAs. One can see very clearly that the EIT peak has split.

This is exactly the principle that we would want to use at IISc. Here, we have obtained EIT signals for upto n$\simeq$ 60. We have also calculated the difference in energy of the Rydberg levels, and the Rabi frequencies of control required to show the transition for a probe power of 50 µW. However, the microwave horn that we have, can only support frequencies upto 6 GHz. This can only be obtained at levels n$\simeq$ 70. The laser diode for the control operates optimally at frequencies lower than this required frequency. As a result, we are not able to go this high in frequency and are severely limited in the power at this high a frequency. Here, we are not using an SHG cavity like in Mainz, which is a better way to produce the blue laser light.

The entire idea behind squeezing is that we exploit the nonlinearities in the Rydberg Blockade and make the EIT probe beam pass through the Rydberg blockade in its entirety, or as much as possible. The Rydberg Blockade scaling is shown in (Fig. 4.16). We have used the Alkali Rydberg Calculator (ARC) package for these calculations. As one can see, the blockade size is around 11 microns only at $n = 82$. We have focused our beam to a **waist of 11 microns** by using 50 mm focal length lenses. Two pairs of lenses are used-for focusing and defocusing. To make the waist comparable to the blockade radius, we need to at least operate at n $\simeq$ 80.

4.5 Observing phase-dependent noise at high n levels

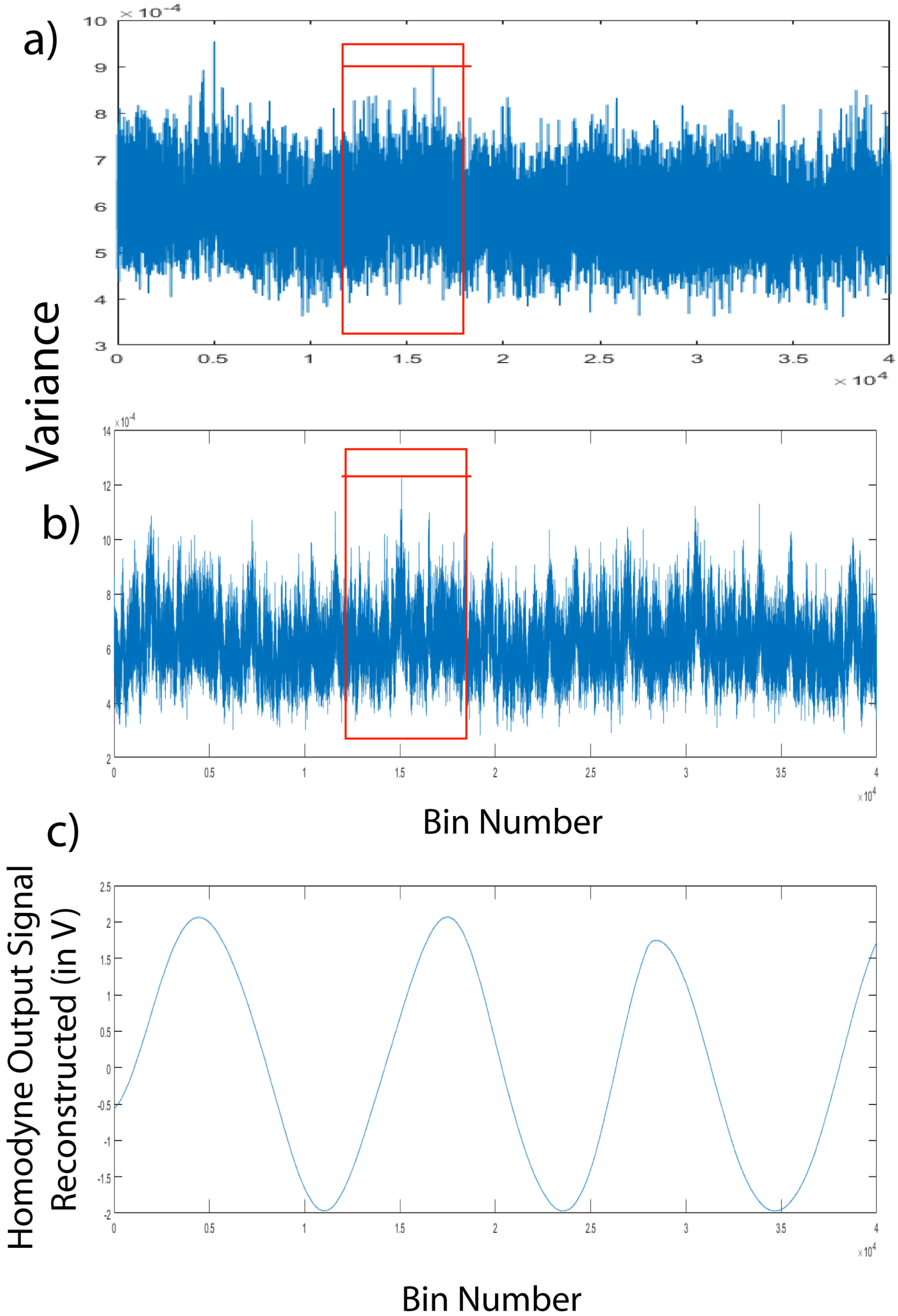

Figure 4.17: Comparison between variance values for squeezed light and for coherent light for $n = 75$. a) Variance as a function of the bin number for coherent light not passed through an EIT. b) Variance as a function of bin number for EIT probe beam obtained after passing through a Rydberg blockade. c) The reconstructed homodyne signal obtained by taking average of data in every bin.

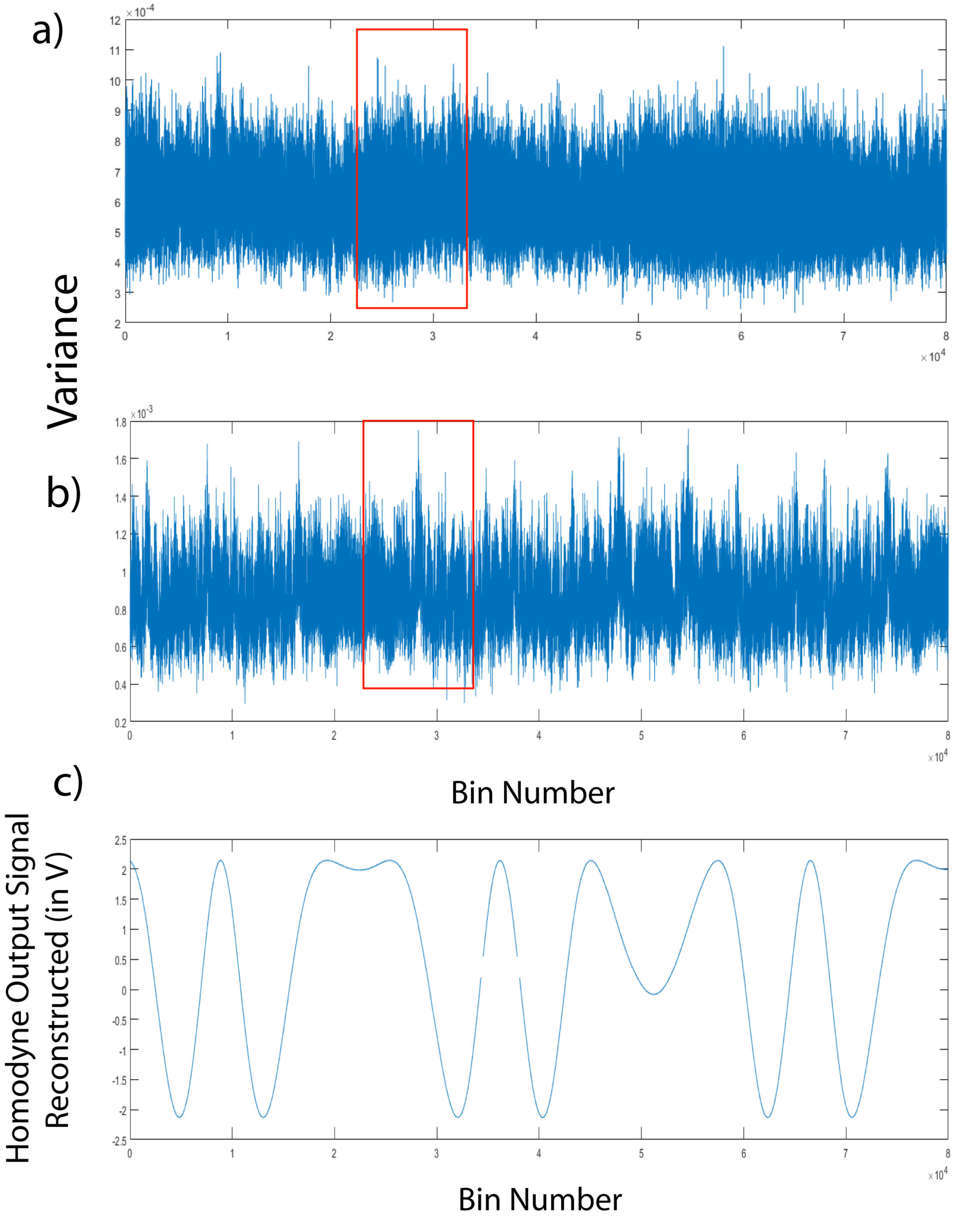

Figure 4.18: Comparison between variance values for squeezed light and for coherent light for $n = 85$. a) Variance as a function of the bin number for coherent light not passed through an EIT. b) Variance as a function of bin number for EIT probe beam obtained after passing through a Rydberg blockade. c) The reconstructed homodyne signal obtained by taking average of data in every bin.

Any signature of squeezing would be associated with phase-dependent fluctuations in the noise level, which would increase from the coherent state shot noise level for certain phase values corresponding to a certain quadrature, where there is anti squeezing. For other phase values corresponding to the other quadrature, the noise level would decrease below the shot noise level, and the decrease is exactly the amount of squeezing that one observes. So there would be alternate peaks and valleys [31]. If at all there is any squeezing or anti squeezing, the variance of the trace from the homodyne setup would show that. (Fig. 4.17) and (Fig. 4.18) show this.

So we have optimised our setup to operate at very high n levels at this point. We have focused our beams to waist sizes comparable to the Rydberg blockade size. We have made our blockades big enough, at least theoretically. We also have observed and locked our lasers to EITs at these high n levels. Turns out, it was indeed fruitful. The first signs of a phase dependent noise appeared around $n = 75$. Notice that the variances without EIT are rather flat while the one with EIT has peaks appearing at certain values of the phase. This becomes more prominent at $n = 85$. The peaks are double in height, meaning that the anti-squeezing is almost 3 dB, if this is anti-squeezing indeed. In essence, we have observed an increase in our noise level upto 3 dB which is only observed at certain phase values. Whether this is indeed anti-squeezing or not, is under further investigation. We have a lot of acoustic noise in our setup, which appears as ripples in the trace obtained from the Homodyne setup. This creates a lot of noise in our graphs of variance. Although phase dependent noise is very clearly visible, we cannot really say what is the value of the squeezing if any, or what is the lowest point in the variance graph. This is a rather elaborate project and this is a very preliminary but first sign of phase dependent noise.

4.6 Future directions

We can identify some improvements in our setup

- Use a voltage amplifier to obtain more cycles per piezo scan and see the repeatability of results.
- Treat the Rydberg EIT as a non-linear medium and use a second probe beam for the squezing detection like one would in say an optical parametric oscillator.
- Sound-proof the setup with foam-lined box.
- Analyse polarisation noise and reduce the loss in EIT arm after mixing PBS.
- Lock the blue laser with a cavity to obtain better locking linewidth.

For the project at IISc, we are primarily limited by our microwave horn. Once we buy a new microwave horn which can support higher frequencies, we will be able to hopefully achieve what we are trying to do.

Bibliography

[1] M. Fleischhauer, A. Imamoglu, and J. P. Marangos, "Electromagnetically induced transparency: Optics in coherent media," *Reviews of Modern Physics*, vol. 77, no. 2, pp. 633–673, 2005.

[2] D. Shylla, E. O. Nyakang'o, and K. Pandey, "Highly sensitive atomic based mw interferometry," *Scientific reports*, vol. 8, no. 1, p. 8692, 2018.

[3] S. Khan, *Experimental Studies in Quantum Optics using Diode Lasers.* PhD dissertation, Indian Institute of Science, Bangalore, 2019.

[4] P. Priyadarsi, *STUDY OF CPO RESONANCE IN THE D2 LINES OF RUBIDIUM 87.* Bachelor thesis, Indian Institute of Science, Bangalore, 2018.

[5] C. J. Foot *et al.*, *Atomic physics*, vol. 7. Oxford University Press, 2005.

[6] V. Natarajan, *Modern atomic physics.* CRC Press, 2015.

[7] M. Fox, *Quantum optics: an introduction*, vol. 15. OUP Oxford, 2006.

[8] M. O. Scully and M. S. Zubairy, "Quantum optics," 1999.

[9] T. Opatrnỳ and K. Mølmer, "Spin squeezing and schrödinger-cat-state generation in atomic samples with rydberg blockade," *Physical Review A*, vol. 86, no. 2, p. 023845, 2012.

[10] O. Firstenberg, C. S. Adams, and S. Hofferberth, "Nonlinear quantum optics mediated by rydberg interactions," *Journal of Physics B: Atomic, Molecular and Optical Physics*, vol. 49, no. 15, p. 152003, 2016.

[11] A. Grankin, *Theoretical studies of optical non-linear effects in ultracold Rydberg gases.* PhD thesis, Université Paris-Saclay, 2016.

[12] A. Bhowmick, D. Kara, and A. K. Mohapatra, "Study of rydberg blockade in thermal vapor," *arXiv preprint arXiv:1802.06599*, 2018.

[13] D. Mills and E. Burstein, "Polaritons: the electromagnetic modes of media," *Reports on Progress in Physics*, vol. 37, no. 7, p. 817, 1974.

[14] A. Mohapatra, T. Jackson, and C. Adams, “Coherent optical detection of highly excited rydberg states using electromagnetically induced transparency,” *Physical review letters*, vol. 98, no. 11, p. 113003, 2007.

[15] O. Firstenberg, T. Peyronel, Q.-Y. Liang, A. V. Gorshkov, M. D. Lukin, and V. Vuletić, “Attractive photons in a quantum nonlinear medium,” *Nature*, vol. 502, no. 7469, p. 71, 2013.

[16] R. Grimm, M. Weidemüller, and Y. B. Ovchinnikov, “Optical Dipole Traps for Neutral Atoms,” *Advances in Atomic, Molecular and Optical Physics*, vol. 42, no. C, pp. 95–170, 2000.

[17] D. Schrader, S. Kuhr, W. Alt, M. Müller, V. Gomer, and D. Meschede, “An optical conveyor belt for single neutral atoms,” *Applied Physics B: Lasers and Optics*, vol. 73, no. 8, pp. 819–824, 2001.

[18] S. Vorrath, S. A. Möller, P. Windpassinger, K. Bongs, and K. Sengstock, “Efficient guiding of cold atoms through a photonic band gap fiber,” *New Journal of Physics*, vol. 12, 2010.

[19] S. Schmid, G. Thalhammer, K. Winkler, F. Lang, and J. H. Denschlag, “Long distance transport of ultracold atoms using a 1D optical lattice,” *New Journal of Physics*, vol. 8, pp. 0–15, 2006.

[20] M. Langbecker, M. Noaman, N. Kjærgaard, F. Benabid, and P. Windpassinger, “Rydberg excitation of cold atoms inside a hollow-core fiber,” *Physical Review A*, vol. 96, no. 4, pp. 1–7, 2017.

[21] M. J. Collett, R. Loudon, and C. W. Gardiner, “Quantum theory of optical homodyne and heterodyne detection,” *Journal of Modern Optics*, vol. 34, no. 6-7, pp. 881–902, 1987.

[22] J. Ding, B. Hou, and S. Wang, “Squeezing survival and transfer in single and double electromagnetically induced transparency,” *Journal of Physics B: Atomic, Molecular and Optical Physics*, vol. 43, no. 22, p. 225502, 2010.

[23] A. Dantan, M. Pinard, and P. R. Berman, “Eit-assisted atomic squeezing,” *The European Physical Journal D-Atomic, Molecular, Optical and Plasma Physics*, vol. 27, no. 2, pp. 193–199, 2003.

[24] Y. Li, Z. Li, D. Wang, J. Gao, and J. Zhang, “Manipulation of squeezed state in electromagnetically induced transparency system via dynamic stark effect,” *JOSA B*, vol. 29, no. 11, pp. 3177–3182, 2012.

[25] C. F. McCormick, V. Boyer, A. M. Marino, E. Arimondo, and P. D. Lett, “Strong relative intensity squeezing by 4-wave mixing in rb vapor,” in *2007 Quantum Electronics and Laser Science Conference*, pp. 1–2, IEEE, 2007.

[26] D. Chruściński and S. Pascazio, “A brief history of the gkls equation,” *arXiv preprint arXiv:1710.05993*, 2017.

[27] S. Khan, M. P. Kumar, V. Bharti, and V. Natarajan, "Coherent population trapping (cpt) versus electromagnetically induced transparency (eit)," *The European Physical Journal D*, vol. 71, no. 2, p. 38, 2017.

[28] S. Khan, V. Bharti, and V. Natarajan, "Role of dressed-state interference in electromagnetically induced transparency," *Physics Letters A*, vol. 380, no. 48, pp. 4100–4104, 2016.

[29] S. Chelkowski, *Squeezed Light and Laser Interferometric Gravitational Wave Detectors*. PhD thesis, Hannover U., 2007.

[30] Y. Ben-Aryeh, "The use of squeezed states and balanced homodyne for detecting gravitational waves," *arXiv*, 2010.

[31] G. Breitenbach, S. Schiller, and J. Mlynek, "Measurement of the quantum states of squeezed light," *Nature*, vol. 387, no. 6632, p. 471, 1997.

[32] I. Friedler, D. Petrosyan, M. Fleischhauer, and G. Kurizki, "Long-range interactions and entanglement of slow single-photon pulses," *Physical Review A*, vol. 72, no. 4, p. 043803, 2005.

[33] J. D. Pritchard, D. Maxwell, A. Gauguet, K. J. Weatherill, M. Jones, and C. S. Adams, "Cooperative atom-light interaction in a blockaded rydberg ensemble," *Physical review letters*, vol. 105, no. 19, p. 193603, 2010.

[34] D. Jaksch, J. Cirac, P. Zoller, S. Rolston, R. Côté, and M. Lukin, "Fast quantum gates for neutral atoms," *Physical Review Letters*, vol. 85, no. 10, p. 2208, 2000.

[35] T. Wilk, A. Gaëtan, C. Evellin, J. Wolters, Y. Miroshnychenko, P. Grangier, and A. Browaeys, "Entanglement of two individual neutral atoms using rydberg blockade," *Physical Review Letters*, vol. 104, no. 1, p. 010502, 2010.

[36] Q.-Y. Liang, A. V. Venkatramani, S. H. Cantu, T. L. Nicholson, M. J. Gullans, A. V. Gorshkov, J. D. Thompson, C. Chin, M. D. Lukin, and V. Vuletić, "Observation of three-photon bound states in a quantum nonlinear medium," *Science*, vol. 359, no. 6377, pp. 783–786, 2018.

[37] J. Giordmaine and R. C. Miller, "Tunable coherent parametric oscillation in linb o 3 at optical frequencies," *Physical Review Letters*, vol. 14, no. 24, p. 973, 1965.

[38] U. L. Andersen, T. Gehring, C. Marquardt, and G. Leuchs, "30 years of squeezed light generation," *Physica Scripta*, vol. 91, no. 5, p. 053001, 2016.

[39] A. B. Matsko, I. Novikova, G. R. Welch, D. Budker, D. F. Kimball, and S. M. Rochester, "Vacuum squeezing in atomic media via self-rotation," *Physical Review A - Atomic, Molecular, and Optical Physics*, vol. 66, no. 4, p. 10, 2002.